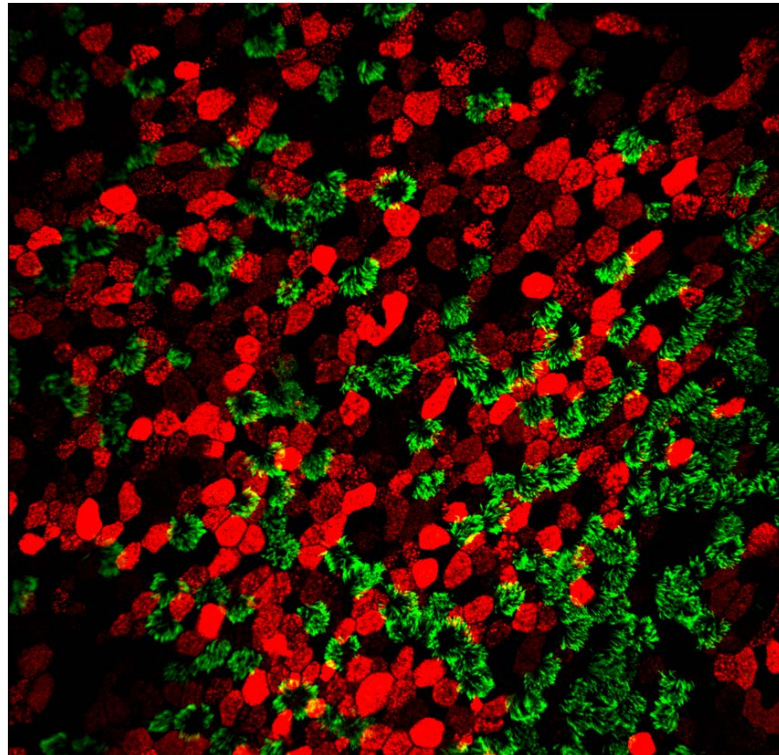# CHALMERS

Wound healing in an *in vitro* bronchial epithelial cell model

Master of Science Thesis

ANDREAS CARLSSON

Department of Applied Physics
Division of Biological Physics
CHALMERS UNIVERSITY OF TECHNOLOGY
Gothenburg, Sweden, 2013

Wound healing in an *in vitro* bronchial epithelial cell model

ANDREAS CARLSSON

Wound healing in an *in vitro* bronchial epithelial cell model
ANDREAS CARLSSON

Cover: Primary normal human bronchial epithelial cell culture immunofluorescent stained for mucin (MUC5AC, red staining) and cilia (TUBB4, green staining). Image captured by confocal microscopy, magnification 40x.

Göteborg, Sweden 2013

Wound healing in an *in vitro* bronchial epithelial cell model
ANDREAS CARLSSON
Department of Applied Physics
Chalmers University of Technology

Abstract

The aim of this project was to investigate the potential use of differentiated primary human bronchial epithelial cells in air liquid interface as a model for wound healing *in vitro*. Wounds were simulated by mechanical scratching and whole cigarette smoke exposure. The outcome of the project is aimed to increase the knowledge of primary bronchial epithelial cells in the respiratory research, the ability to use the model for wound healing studies and the potential use of the model for compound testing. The primary read-outs used to evaluate the model were real-time quantitative polymerase chain reaction, immunocytochemistry, live imaging, image analysis and trans epithelial electrical resistance.

From this project primary human bronchial cell cultures were concluded to have a high recovery potential to both scratch wounds and exposure of whole cigarette smoke. The wound healing results obtained from this project were connected to previous described theories of *in vivo* wound healing and the major cell populations were observed to recover over time. Cigarette smoke was observed to significant delay the wound healing of scratch wounded cell cultures, a feature used to investigate pharmaceutical compounds effect to migration in the cell model. Treatment of three different compounds to the model in this project did not show any effect to the cell migration. Live imaging of scratch wounded cell cultures revealed a migration within the whole cell culture during wound healing. Surprisingly, non-wounded fully differentiated cell cultures showed a constant cellular migration which, as to the writer's knowledge, has not been previous reported.

Through this project a successful wound healing model was established using a combination of read-outs. A model for cigarette smoke exposure of air liquid interface cultures was performed and a window for compound treatment was discovered as a result of the impact of cigarette smoke on cellular migration.

This project was performed in collaboration between Chalmers University of Technology and AstraZeneca R&D, at the section of Cell and Molecular Pharmacology within the department of Respiratory, Inflammation and Autoimmunity at AstraZeneca R&D facility in Mölndal.

Keywords: Primary normal human bronchial epithelial cells, air liquid interface, wound healing, ICC, real-time qPCR, live imaging, confocal microscopy, cigarette smoke.

Abbreviations

ALI   Air liquid interface

cDNA   Complementary DNA

CF   Cystic fibrosis

COPD   Chronic obstructive pulmonary disease

CPSS   Clara cell secretory protein

CSC   Cigarette smoke condensate

CSE   Cigarette smoke extract

DAPI   4',6-diamidino-2-phenylindole

DMEM   Dulbecco's Modified Eagle's Medium

ECM   Extracellular matrix

DNA   Deoxyribonucleic acid

HBEC   Human bronchial epithelial cells

ISO   International Standards Organization

MMP   Matrix metalloproteinase

mRNA   Messenger RNA

NHBE   Normal human bronchial epithelial

PBS   Phosphate-Buffered Saline

RNA   Ribonucleic acid

ROI   Region of interest

TEER   Trans epithelial electrical resistance

ZO   Zonula Occludens

Contents

1   Introduction

Today there are a number of respiratory diseases causing suffering and death by the human population. Global health issues such as chronic obstructive pulmonary disease (COPD), asthma and cystic fibrosis (CF) are some of them. COPD caused 5% of the global deaths in 2005 and estimations suggests that in the year of 2004, 64 million people worldwide were suffering from COPD. Prediction made by the World Health Organization (WHO) predicts COPD alone to become the third leading cause of deaths by 2030 [1, 2]. Asthma, another global respiratory disease less lethal compared to COPD, are the largest non-communicable disease seen among children. Estimations suggest that 235 million people suffers from asthma around the world today. Patients diagnosed with bronchial asthma have shown presence of epithelial shedding in the airways, a condition causing disruption of the apical epithelial cell layer from the basal membrane, resulting in wounds and loss of epithelial integrity. Regardless of respiratory disease, a common consequence is that the airway epithelium is exposed to damage or unfavourable condition which eventually can cause harm to the respiratory system. Observations by both asthmatics and COPD patients reveals a common feature of epithelium damage causing chronic inflammation and hyperresponsiveness [3].

In order to assess disease stages associated with respiratory diseases such as asthma and COPD, development of new and refining of existing *in vitro* models are of interest in the early development of pharmaceuticals. Although existing animal models are used in the respiratory research, there are issues introducing respiratory diseases to them. By the human complexity, the human heterogeneity cannot be reflected in existing animal models [4]. Development of new *in vitro* models, reflecting an *in vivo* state, could benefit the development of new drugs to respiratory diseases. Using complex cell systems could potentially reduce and to some extent replace animal testing by refinement of new upcoming compounds in drug discovery.

Through this project, primary normal human bronchial epithelial (NHBE) cell cultures have been cultured in an air liquid interface (ALI) in order to use fully differentiated airway epithelial cells, expressing both mucins and functional cilia, to evaluate a model for wound healing *in vitro*. The evaluated wound models were simulated by mechanical scratching and exposure of whole cigarette smoke. The ALI cultures has been documented stable over time [5], suggesting the possibility of monitoring the wound healing over time. In this project several readouts such as real-time quantitative polymerase chain reaction (real-time qPCR), live imaging, immunocytochemistry (ICC), image analysis and trans epithelial electrical resistance (TEER) were used to follow the wound healing.

1.0.1   Aim

The aim of the project was to establish and evaluate a wound healing assay reflecting the bronchial epithelium of human airways. The wounds and damages to the epithelial cell cultures were simulated by two methods, mechanical scratching and exposure of whole cigarette smoke. Establishing a scratch assay, migration and proliferation could be monitored, simulating wound healing. Establishing a protocol for exposure of whole cigarette smoke could promote investigation of the damage to the cell cultures caused by the cigarette smoke.

In order to analyse the models, multiple analysis methods were evaluated. This work included establishing functional protocol for ICC, including evaluations of multiple antibodies for analysis of protein expression. Additional analysis methods evaluated were the performance of live imaging, measurement of TEER and measurement of gene expressions by real-time qPCR. Using ALI cultures of NHBE cells, capable of expressing both mucins and functional cilia, a more *in vivo*-like model was assessed compared to existing submerged monolayer cultures. This model could serve as a refined model, for the development of new pharmaceuticals intended for distribution though the respiratory system, before entering animal testing.

1.0.2   Outline

The project was divided into four parts; method evaluation, scratch assay, smoke assay and compound treatment. The initial part consisted of evaluating methods used in the project followed by evaluation of scratch assay and smoke assay. In the last part of the project, initial trials was performed assessing the effect of three in house AstraZeneca compounds using the scratch assay. Compound A and B have previous shown toxic effect in dog airway epithelium *in vivo*. Through this initial trial the outcome results could be compared against previous reported *in vivo* data. A positive control substance C was assessed as well to compare any impact of the different compounds.

This project was performed during one year through a collaboration between Chalmers University of Technology and AstraZeneca R&D, performed at the section of Cell and Molecular Pharmacology within the department of Respiratory, Inflammation and Autoimmunity at AstraZeneca R&D facility in Mölndal.

1.0.3 AstraZeneca

AstraZeneca, a global biopharmaceutical company operating in over 100 countries, specialising in discovery, development, manufacturing and marketing of medicines within six areas of health care: cardiovascular, gastrointestinal, infection, neuroscience, oncology and respiratory and inflammation. The product portfolio of AstraZeneca contains products within all six areas, such as Symbicort® and Pulmicort® within the health care area for respiratory and inflammation. AstraZeneca was formed through the merge of the Swedish company Astra AB and the UK based company Zeneca Group PLC in 1999, with the headquarters today located in London UK. Today AstraZeneca has approximately 51'700 employees world wide and recorded a revenue of $27.97 billions by 2012 [6].

2   Theory

2.1   Human airway

The human airway is divided into two major parts; upper- and lower respiratory system. The upper respiratory system consists of the nasal cavity and the pharynx, the lower respiratory system of the larynx, trachea, bronchi, respiratory bronchioles and alveolar ducts, see figure 1. The trachea, as well as the initial part of the bronchi, is composed of a protective mucous membrane and a pseudostratified columnar epithelium, consisting of three cell types; ciliated cells, goblet cells and basal cells, see figure 2. In the lower part of the bronchi, the cell composition is changed and forms a non-ciliated simple cuboidal epithelium containing ciliated cells, Clara cells and basal cells. The most distal part, the alveolar duct, is composed of simple squamous epithelial cells consisting of alveolar type I and type II cells [7, 8].

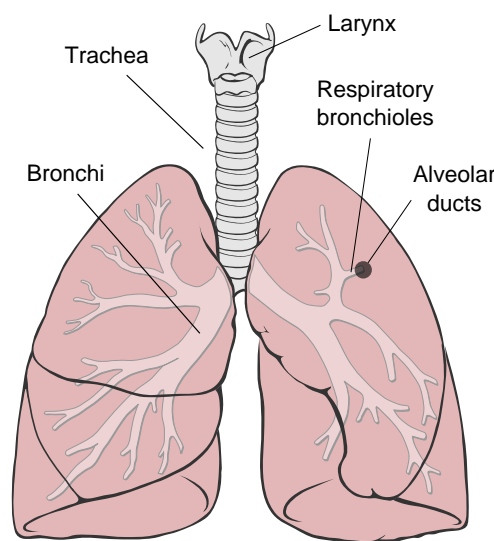**Figure 1:** Illustration of the branching of the human airway, from the larynx to the alveolar ducts. Modified image adapted from Patrick J. Lynch, medical illustrator, http://en.wikipedia.org/wiki/File:Lungs_diagram_simple.svg, uploaded 4 August 2010.

The epithelium, found lining the human airways, is one of the basic tissues in humans forming the epidermis and lining the digestive and genitourinary system.

Its function in the respiratory system is to serve as a barrier between the outer environment and the underlying tissue. Two striking features of epithelium are the formation of tight junctions and its cell polarization. Depending on location, the epithelium is divided into different classes based on the morphology. The trachea and bronchi are composed of a pseudostratified columnar epithelium [8, 9], characterized by a cell sheet where all cells have contact with the basement membrane and some of the cells reaches the epithelium surface while others do not, see figure 2 [9].
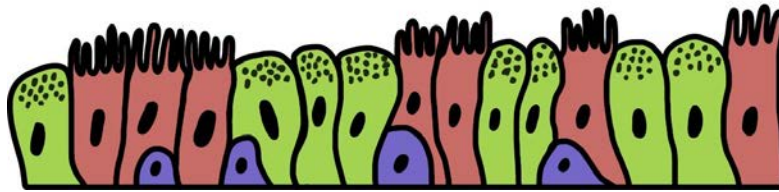
Figure 2: Illustration of a pseudostratified columnar epithelium seen in trachea and bronchi, consisting of three cell types; ciliated cells (marked as red cells), basal cells (marked as blue cells) and goblet cells (marked as green cells with black dots representing the mucins).

2.1.1   Mucus producing cells

The protecting mucus membrane, or mucus layer, located in the airway is secreted by two different cell types, goblet cells located at the surface epithelium and mucous cells located in the submucosal glands [10]. The goblet cell is located in both the upper and the lower respiratory system where approximately 25% of the cells forming the bronchial epithelium are goblet cells in humans. The goblet cell primary function is to produce mucins, heavy glucosylated proteins, onto the epithelial surface to form a liquid layer, up to 50 µm thick. This layer, known as mucus, is in healthy persons composed of 97% water and 3% solid particles in form of mucins, salts, lipids, cellular debris and other proteins. The mucus is designed to trap foreign particles, viruses and other toxins and by ciliary beating and coughing transport it out of the respiratory system. The removal of mucus through cilia beating is known as mucociliary clearance, where mucus from the upper respiratory system is transported down to the pharynx and mucus from the lower respiratory system is transported up to the pharynx where it is swallowed or spitted out. Large amounts of mucus is produced daily and approximately 30 ml of mucus is swallowed every day in healthy humans. There are seventeen genes found encoding for human mucin proteins, where MUC5AC is produced mainly by the goblet cell and MUC5B mainly by the submucosal gland [8, 11, 12].

2.1.2 Ciliated cells

The mucociliary clearance performed by ciliated cells are found in the upper respiratory system, down to the start of the respiratory zone where the gas exchange is performed. The transport of mucus is performed through cilia beating, a coordinated movement performed in the same direction with about 12 beats per second [13]. Ciliated cells express clusters of approximately 200 motile cilia, each with a length of about 7 μm and a diameter of 0.2-0.3 μm, at the cell surface towards the airway [11, 14, 15]. The cilia is a microtubule organelle consisting of tubulin, a structural protein with equal amounts of α and β monomers. There are seven different β-tubulins in mammals, β_I, β_{II}, β_{III}, β_{IVa}, β_{IVb}, β_V and β_{VI}, where the cilia found in tracheal epithelium have the specific β_{IV} isotype [16–18]. β_{IV} (TUBB4) is expressed as a cytoskeletal protein as well and has successfully been used to stain and visualize the cilia of cultured airway epithelial cells [19].

The cilia is divided into two classes; primary and motile cilia, where motile cilia has a functional movement in order to transport fluids, such as mucus in the airways or fluids in the fallopian tubes and brain ventricles. Primary cilia is nonmotile and its functions is still not fully understood, but hypothesised to act as chemical and mechanical sensors [20]. Observations suggests motile ciliated cells to originate from primary ciliated cells, where the transcription factor FOXJ1 has been identified to control the formation of motile cilia [14, 21].

The sperm, another cell type containing a functional motile organelle, has shown to contain a specific protein present in ciliated cells. Sperm protein 17 (SP17), found in both sperm and testis, has shown to be present in ciliated cells from *in vivo* tissue samples of the larynx, trachea and lungs as well as in *in vitro* cultured airway epithelial cells [22, 23].

2.1.3 Progenitor cells

Depending of location in the human airway, different cell types are hypothesised to act as the progenitor cell type. In the upper airway, in the trachea and large bronchi, located below the goblet and ciliated cells in the border to the basement membrane, the basal cells are found. The basal cell, expressing tumour protein 63 (p63), are thought of being the progenitor cell type responsible for proliferation and differentiation of goblet and ciliated cells [24, 25]. Further down the small airway, in the lower part of the bronchi the Clara cells are thought of acting as the progenitor cell type [26]. Clara cells are a non-ciliated cell with the capability of secreting a surfactant, Clara cell secretory protein (CCSP), to the airway epithelium [27]. In the most distal parts of the lung, the alveolar epithelium are thought to have

their own progenitor cell type, the type II alveolar epithelial cell, which is able to differentiate into type I alveolar cells [24].

In order to study cellular proliferation expression of several proliferation proteins can be used, such as the KI-67 protein [28, 29] and the proliferating cell nuclear antigen (PCNA) protein [29], both detected in the nucleus of proliferating cells. KI-67 has shown to be expressed throughout the active phase of cell cycle (G_1, S, G_2 and mitosis) [28] while PCNA, together with DNA polymerase δ, is active during the cell cycle of proliferation [29].

2.1.4   Basement membrane

Beneath the airway epithelium, the supporting basement membrane is found, composed by a structure of collagen IV, fibronectin, laminin and glycosaminoglycans. Located deeper and further away from the epithelium, the composition of the basement membrane is changed to mainly contain collagen III. The thickness of the membrane is approximately 10 µm in healthy bronchi [24].

2.1.5   Cell junctions

The apical cells of the epithelium are connected to each other by three different types of junctions; occluding junctions, anchoring junctions and communicating junctions [24]. The occluding junctions, known as tight junctions in vertebrae, forms a barrier separating the outer environment from the basal lamina and seals adjacent cells together forming an impermeable barrier to macromolecules. The two major transmembrane proteins in tight junctions are claudins and occludins. Claudins and occludins can be connected to intracellular proteins known as zonula occludens (ZO) to anchor the proteins to the cytoskeleton [13]. Claudins are responsible for the permeability regulation between cells and occludins are part of the formation of new tight junctions. There are three different zonula occludens; ZO-1, ZO-2 and ZO-3, where ZO-1 activity is associated with high epithelial resistance [30].

Anchoring junctions are mainly divided into two different forms; adherent junctions responsible for cell-cell contacts through transmembrane proteins of the cadherin family and focal adhesions responsible for anchoring the cells to the ECM [13]. The member of cadherin found in epithelial tissue is known as epithelial cadherin, or E-cadherin encoded by the CDH1 gene [31], important for proper tight junction formation of airway epithelial cells [30].

Gap junctions, 2-4 nm wide gaps formed by connexin proteins into small channels, allows transport of inorganic ions and water soluble molecules between cells [13]. Cell-cell signalling through gap junctions in epithelial cells have been seen promoted through mechanical stimulation, initiating Ca^{2+} waves spreading to adjacent cells to promote cell-cell communication [32].

2.2   Airway diseases

Today there are a number of respiratory diseases responsible for suffering and death of the human population such as asthma, COPD and emphysema. COPD is defined as "a preventable and treatable disease state characterized by airflow limitation that is not fully reversible" [33]. The limitation of airflow is associated to an abnormal inflammation response within the lungs, caused by toxic gases or particles. Gases thought as the primary cause of the disease are tobacco smoke as well as risk factors such as pollution from combustion of biomass for indoor heating and cooking, work-related exposure of chemicals and dusts [33, 34]. The complexity of COPD causes it not to be assessed as a single disease, but a group of different diseases including chronic bronchitis and emphysema [8, 35]. Symptoms arising from chronic bronchitis are such as cough, pulmonary hypertension and cyanosis as a response to intense secretion of mucus into the bronchi. Emphysema is caused of impaired oxygen uptake as a response to the destruction of the epithelium of the alveoli [8].

Asthma is classified a chronic respiratory disease characterized by inflammation and sensitivity to stimulus of different allergens causing airway hypersensitivity. Symptoms of swelling in the bronchi is also observed causing a reduction of airflow to the lungs as a response to excessive mucus production or damage to the epithelium [8]. Asthma is, compared to COPD, not considered as deadly and can be medicated to control inflammation and to suppress the swelling of the airways [36].

2.2.1   Damage to the epithelium

The airway epithelium serves as the first line of defence and protects the airway against inhaled particles, pathogens and toxic chemicals [11]. The respiration causes a constant exposure of potential dangerous materials such as toxic agents, microorganisms, viruses and pollutants as a healthy human inhales approximately 12'000 litres of air every day [12]. Independent of the source of injury, caused by diseases or inhalation, the response could result in loss of epithelium integrity,

shedding of the epithelium or total denudation of the basal membrane [37]. Disruption of epithelium from human airway have been observed in bronchial asthmatics showing presence of epithelial shedding. The injury of the shedding has shown to be superficial as the shedding mainly contains columnar epithelial cells with low amounts of basal cells, suggesting a disruption of goblet and ciliated cells [38].

2.2.2 Cigarette smoke impact

Not only does chronic exposure of cigarette smoke causes diseases such as COPD and bronchitis, but low doses can be seen promoting negatively signals in human. Cigarette smoke affects the respiratory system by narrowing the airways which reduces the amount of oxygen reaching the lungs. The obstruction reduces the uptake of oxygen as well as the hemoglobin efficiency. At cellular level the smoke affects the mucus producing cells by increase of mucus production and release [8, 39, 40], destroying the cilia causing impairment of the mucociliary clearance [8], decrease expression of epithelial cadherin [41] and induce disassembly of thigh junction proteins ZO-1 and occludin as well as delays the formation of new tight junctions [42]. *In vitro* studies of airway epithelial cells exposed to cigarette smoke have shown large stress responses such as increase levels of heat shock protein 70 kDa (HSP70B or HSPA6), DNA-damage-inducible transcript 3 (DDIT3) and thioredoxin reductase 1 (TXNRD1) [43]. Inflammatory responses from cigarette smoke have been observed by increased levels of cytokines, such as interleukin-6 (IL-6) and IL-8 [44]. IL-8 is released as a response to inflammatory stimuli, such as cigarette smoke [45], causing accumulation of neutrophils to the exposed area [46]. Cigarette smoke has also shown to negatively affect the cellular proliferation [47].

2.3 Airway wound healing

The specific wound repairing processes of airway epithelium are today not fully understood. Several methods, such as implanting human xenografts in nude mice have been used to study the wound healing processes [48]. Suggested processes of wound healing, can for simplicity be divided into four major steps; dedifferentiation, migration, proliferation and redifferentiation [49], see figure 3. Upon an injury to the epithelium an acute inflammatory response is initiated and immune cells are located to the injured area. Cytokines, chemokines and growth factors are released in the area, as a part of the healing process, together with other factors to promote cell migration [50]. The cells next to the wound edge starts to dedifferentiate and migrate, in order to cover the denuded wound area and establish a

confluent layer of undifferentiated cells. Once the wound is covered, cells in the wound area starts to proliferate forming a cuboidal stratified cell layer which, as the healing continuous, changes and forms into a pseudostratified cell layer. The last step in the healing process involves redifferentiation of the undifferentiated cells, establishing a fully functional epithelium [48, 49].
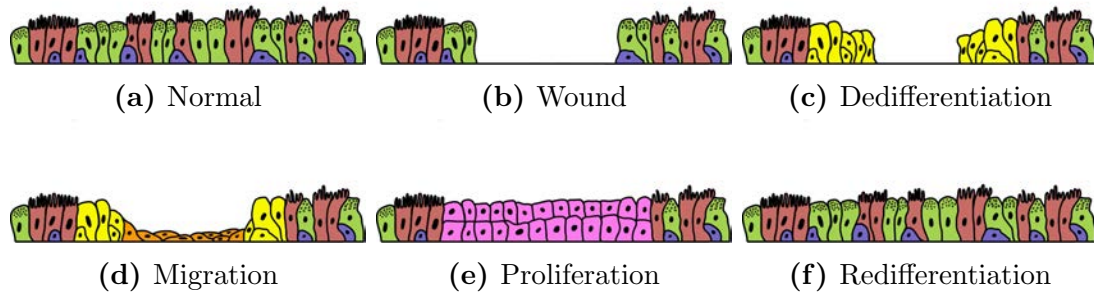

(a) Normal   (b) Wound   (c) Dedifferentiation

(d) Migration   (e) Proliferation   (f) Redifferentiation

Figure 3: Epithelial wound healing illustrated through four steps. As a normal epithelium is introduced to a wound, cells adjacent to the wound edge will start to dedifferentiate (cells shown in yellow) and migrate (cells shown in orange) to the wounded area to form an epithelial barrier to the underlying tissue. Once the wound area is covered, cells will start to proliferate (cells shown in pink) and finally redifferentiate to establish a fully functional epithelium.

The cellular migration seen in wound healing have been linked to MMP-9, a matrix metalloproteinase (MMP), in airway epithelium. *In vitro* studies suggest involvement of MMP-9 to the migration and differentiation during re-epithelization of the airway epithelium [48]. MMPs, a family of extracellular endopeptidases originally considered as a family of extracellular enzymes controlling the degradation of ECM, possesses the ability to alter the affinity of cell-cell interactions. MMP-9 is considered to be a weak collagenase and involved in promoting cell migration in airway epithelium [51]. *In vitro* studies of both HBEC and human nasal epithelial cells (HNEC) reveals an increased expression of MMP-9 during wound healing. The increased levels of MMP-9 has predominant been observed in migrating cells adjacent to wound edges [52, 53].

2.4   *In vitro* models

To assess disease stages associated with respiratory diseases, the development of new and refinement of existing *in vitro* models are of interest. Today the existing

animal models used in respiratory research suffers the ability to introduce diseases such as COPD and asthma on to them.

2.4.1   Cell cultures

To assess problems and investigate disease stages *in vitro*, different cell models are available from different areas of the respiratory tract. Cell cultures available for modulating the respiratory regions are found from the of nasal, tracheal, bronchial and alveolar area. Cell cultures are available both as immortalised cell lines and as primary cells. Bronchial epithelial cells available as immortalised cell lines are such as Calu-3 (carcinoma cells), 16HBE14$^-$ (transformed cells) and BEAS-2B cells (transformed cells). Primary cells are found as NHBE cells from healthy donors as well as epithelial cells from COPD and asthmatic donors. Depending on experimental design, nasal, tracheal and bronchial epithelial cells can be cultured in an air liquid interface to mimic more *in vivo* like conditions [54].

The use of primary cells or immortalized cell lines has both benefits and limitations. Primary cells has the advantage of a closer representation of an *in vivo* situation, expressing both mucus producing cells and functional cilia in combination of high TEER values and consistent mRNA and protein expressions. The variation between cell donors, cell passage and experiments leads to the need of stable protocols. The primary cells are more expensive, harder to manipulate and accesses a limited cell source compared to immortalized cell lines. [19, 55].

Mimicking the *in vivo* situation, using *in vitro* models, ALI cell cultures possesses multiple benefits as a model. ALI cultures of human bronchial epithelial cells are able to differentiate and mature, containing large amounts of functional ciliated cells [22], goblet cells producing mucus onto the air milieu and basal cells. Epithelial cells are initially seeded in a submerged condition and transferred to an air liquid interface once the cells are confluent, see figure 4. The exposure of air to the cells, in combination with retionic acid containing culture medium, triggers the differentiation of different cell types, formation of tight junctions and pseudostratification of the cell layer. Compared to submerged monolayer cultures, ALI cultures possesses a more *in vivo* like state with the ability of aerosol stimulation, with potential of evaluating pharmacological compounds for distrubution through the airway as well as irritants and toxic compounds. ALI cultures also possesses the possibility to culture epithelial cells in co-cultures with other cell types such as fibroblasts or immune cells to promote an even more *in vivo* like model [54].
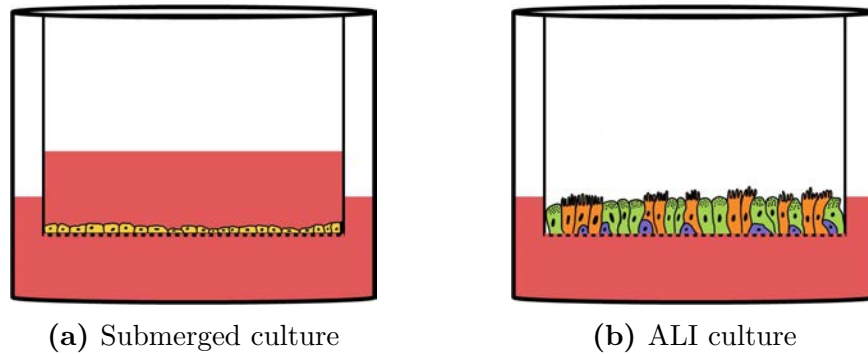
(a) Submerged culture   **(b)** ALI culture

Figure 4: Cultivation of epithelial cells are initially performed in a submerged condition. Once the cells are confluent and covers the growth area to 100%, the culture is transferred to an air liquid interface (ALI) by removal of the apical medium. The exposure of air to the apical compartment triggers the differentiation of the epithelial cells into different cell types, formation of tight junctions and pseudostratification of the cell layer.

The human *in vivo* situation compared to *in vitro* models of airway epithelium have shown large similarities. Investigation of a total of 158 genes connected to ciliated, basal and secretory cells using 358 probe sets showed similar expression profiles to 81% of the expressed genes. ALI cultures showed differences in higher expression of basal cell markers and proliferation markers compared to the *in vivo* samples, which had higher expression of ciliated cell markers and markers connected to the cytoskeleton and immune responses [56].

2.4.2 Wound healing models

Wound healing models of airway epithelial cells have been documented successfully used, with both submerged and ALI cultures. Scratch assays are commonly used to introduce wounds [52, 57–61] as well as other similar techniques such as cell detachment through NaOH exposure [53, 62] and cell removal by high air pressure [63] in order to assess wound healing properties of cell cultures.

2.4.3 Smoke exposure techniques

Models simulating the effects of cigarette smoke to cell cultures have been performed through different techniques. Cigarette smoke, composed of several thousand different components [64], distributed approximately by a 6.5% particle phase and a 93.5% vapour phase [65]. To submerged cell cultures stimulation of cigarette

smoke is commonly distributed through culture medium containing diluted cigarette smoke, either by cigarette smoke extract (CSE) [39–42, 66, 67] or cigarette smoke condensate (CSC) [68, 69]. CSE is usually prepared by bubbling cigarette smoke through culture medium and thereby representing the vapour phase. CSC is prepared by extracting the particulate matter from smoked cigarette in DMSO followed by dilution in culture medium, thereby representing the particle phase. The CSE and CSC are diluted in desirable concentration and used to expose the cell culture during a defined period of time.

Techniques to simulate the behaviour of cigarette smoking more closely to the *in vivo* situation can be performed by exposure of whole cigarette smoke to ALI cultures, using smoking robots such as the Vitrocell VC10 [70] or the Borgwaldt RM20S [71]. A predefined set up, according to International Standards Organization (ISO), 35 ml of smoke is taken during two seconds every one minute to simulate *in vivo* smoking conditions [43, 71, 72]. Smoking machines such as the Borgwaldt RM20S enable the possibility to reproduce smoke exposure experiments over different time periods with specific determined smoke dilutions. The device is automatic and is able to load, light and extract burned out cigarettes, and can be used for chronic and prolonged smoking experiments [72].

2.5   *In vivo* models

In vitro models are often evaluated before experiments are performed in *in vivo* models, using laboratory animals, in the pharmaceutical industry. Animals used as *in vivo* models do possess differences between animals and humans. Lung structure such as the structure of mice, differs from humans as well as the cell composition between the two species. The tracheal epithelial cell structure in mice is composed of large parts of ciliated cells and Clara cells, while the Clara cells are found in the distal bronchial airways in humans. The mucus producing submucosal glands, located both in the upper and lower airways in humans, are present only in the upper parts of the trachea in mice [37]. In healthy humans, the protective mucus layer covering the airway is produced by goblet cells (MUC5AC) and submucosal glands (MUC5B), while in mice almost no Muc5ac is produced. The airways of mice are more similar to the structure of the lower airway in humans [11]. Alternatives to use animal models in more refined ways are through human xenograft models. Using airway epithelial xenografts in mice, the maturation and regeneration of human airway can closely be studied to better understand wound healing [37].

3   Analytical procedures

In order to follow cellular changes through gene expression, protein expression and non invasive techniques, different analysis tools can be adapted. This last theoretical part will describe different available readouts used to investigate cellular behaviour throughout the project.

3.1   Quantification of gene expression

Real-time quantitative polymerase chain reaction (qPCR) was used to evaluate the expression of different genes. To perform qPCR, collected mRNA samples is transcribed into single stranded cDNA through reverse-transcription polymerase chain reaction (RT-PCR). cDNA is used as template to perform qPCR. Adding fluorophore labelled probes, specific to the gene or target sequence of interest, each PCR cycle will cleave a certain amount of fluorophores, emitting light at a specified wavelength. The emitting light is measured when reaching over a predetermine baseline set to separate background noise from a correct signal. If the target sequence is highly expressed in the sample, the emitting light will reach the baseline by fewer PCR cycles compared to a low expressed target, allowing determination in real time during each PCR cycle [73].

In this project, TaqMan assays were used with qPCR to quantify different gene expressions. Based on the Taq polymerase and dual-labelled fluorescent probes, TaqMan assays have been shown to be a fast, reliable and reproducible technique [74].

3.2   Quantification of protein expression

Analysis and quantification of protein expression within cell samples can be adapted by immunocytochemistry techniques. Specific proteins can be targeted and marked with fluorescent labelled antibodies and the fluorescent signal can be measured through image analysis, allowing determination of protein changes over time.

To determine the functionality and specificity of an antibody, all antibodies used in the project were evaluated through immunoperoxidase staining in sectioned epithelial cell cultures. Visual localization of the antibody in the cell culture determined its specificity. Functional antibodies, determined by the evaluation, were later used by immunocytochemistry methods to detect specific proteins in fixated cell cultures. Using image analysis tools to captured images of stained cell cultures,

measurements of percent stained area of each sample could be determined. The cell cultures were seen sensitive to mechanical strain and cells were seen detached from the supporting membrane holding the culture during permanent mounting to microscope glass. To avoid inaccurate measurements of amount stained area, measurements were conducted to different regions of interest (ROI's) within each cell culture to gain more accurate data. The ROI's were manually determined through visual inspection of each cell membrane analysed.

3.3   Trans epithelial electrical resistance

Validating the health of epithelial cell cultures, a non-invasive technique known as Trans Epithelial Electrical Resistance (TEER) was used. The technique relies on measuring the resistance of an electric current travelling across the cell culture. Epithelial cells are linked together by formation of tight junctions, forming an impermeable barrier to macromolecules. The TEER technique uses an electric resistance meeter to measure the electrical resistance between an upper and a lower liquid filled compartment, usually filled with PBS or culture medium, where the membrane containing the epithelial cell culture separates the two compartments [54], see figure 5. The plasma membrane of the epithelial cells has documented high resistance and the measured resistance is reflecting the current travelling through the tight junctions as a result of its ionic permeability [75]. Fully differentiated HBEC cultures expresses tight junctions with high resistance, reaching normal values between 200-1000 $\Omega \cdot cm^2$ [54].
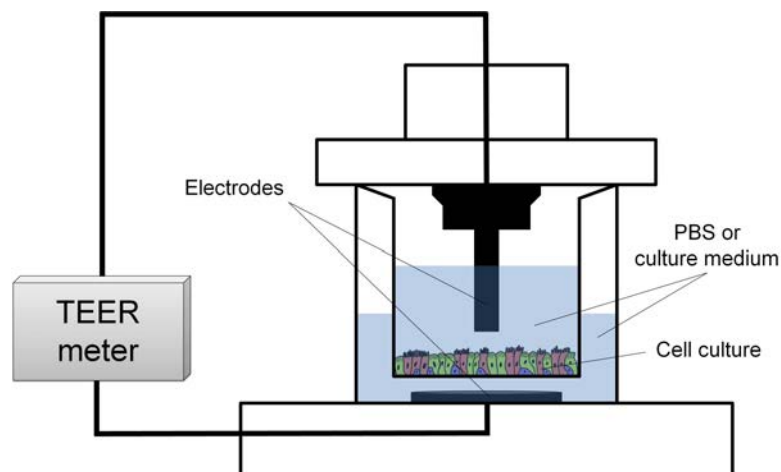
Figure 5: Illustration of the TEER set up. The epithelial cell culture, submerged in PBS or culture medium, is placed between two electrodes during the measurement.

3.4   Live imaging

Live imaging, a non-invasive method, was used to track the cellular migration within the cell cultures. Using the Cell-IQ system (CM Technologies, Tampere, Finland), two culture plates could be monitored simultaneous in a system combining the environment of an incubator with a automated phase-contrast microscopy. The on build software allowed specific areas of interest within the cell cultures to be selected for continuing imaging. Captured images were at a final stage merged into videos to visualize cellular movements and could be analysed to measure cellular migration over time.

4 Materials and methods

The project was, as previous described, divided into four different parts; method evaluation, scratch assay, smoke assay and compound treatment. The method evaluation was conducted in the beginning of the project spanning over a large part of the total work. All methods were evaluated before starting the scratch assay. Following section will describe the materials and methods used during the project.

4.1 Normal human bronchial epithelial cells

Primary NHBE cells (Lonza, Basel, Switzerland) isolated from the epithelial cell layer lining the airway directly above the bifurcation of the lungs were received at passage 1. Three different cell donors were used, see table 1. All donors were screened for cancerous tissue and diseases directly affecting the lungs[1].

Table 1: NHBE cell donors used during the project.

Donor	Batch number	Age	Sex	Race	Smoker
1849	231849	32	Male	Caucasian	No
4449	244449	60	Male	Caucasian	No
12240	4F0786	17	Male	Caucasian	No

4.1.1 Culture conditions

NHBE cells (Lonza, CC-2540), expanded[2] to passage 2 (1'000'000 cells/ml), were seeded on collagen coated, 1:100 volume/volume PureCol (Advanced BioMatrix, 5005-B)/ddH$_2$O, Transwell permeable polyester membrane inserts in 24 well plates (Corning, 3470). Cells were plated at a concentration of 30'000 cells/cm^2 in NHBE medium, a mixture of BEBM (Lonza, CC-3171) and BEGM SingleQuot Kit (Lonza, CC-4175). When reached confluence the immersed culture was transferred, by removal of the apical medium, to an air liquid interface in ALI medium, a mixture of BEBM (Lonza, CC-3171), BEGM SingleQuot Kit (Lonza, CC-4175),

---

[1]Information provided by Lonza.

[2]Passage 1 cells were expanded to passage 2 by Cecilia Forss, Senior Research Scientist, AstraZeneca R&D Mölndal.

1.5 mg/ml BSA (Sigma, A9418), 0.1 mM Retinoic acid (Sigma, R2625), DMEM (Gibco, 41965-039), 100 mM Minimum Essential Medium Sodium Pyruvate (Gibco, 11360-039), 200 mM L-Glutamine (Gibco, 25030-024) and Minimum Essential Medium Non-Essential Amino Acids (Gibco, 11140-035). Lists of media and specific medium content can be seen in Appendix A. Medium was changed every second or third day. In connection to medium change, the produced mucus was gently removed through aspiration. Cell cultures were held in a controlled environment at 37°C, 5% CO_2 and 95% rH during cultivation and were let to differentiate approximately 28 days before experimentation.

4.2   Scratch wounds

Scratch wounds were introduced to cell cultures by scratching with glass Pasteur pipettes connected to 0.6 bar vacuum. Cell debris were removed by washing cultures with 37°C PBS (Gibco, 10010-015).

4.3   Trans epithelial electric resistance measurements

Trans epithelial electrical resistance was monitored with EVOM^2 Epithelial Voltohmmeter (World Precision Instruments Inc., Sarasota, FL, USA) connected to STX2 Chopstick Electrode (World Precision Instruments Inc.) or Endohm 6 mm Culture Cup (World Precision Instruments Inc.). The measurements were conducted adjacent to the medium change to minimize environmental changes for the cell cultures. The devices were, prior to the measurements, cleaned with ethanol and PBS (Gibco, 10010-015). Prior to measurement, cell cultures were washed with 37°C PBS (Gibco, 10010-015), followed by a short incubation (2-3 minutes) in 37°C PBS (Gibco, 10010-015) in both the apical and basolateral compartment. TEER values were collected in triplicates for each culture investigated. To decide the resistance of the cell culture, TEER values were collected in triplicates for a blank Transwell insert containing no cells and subtracted from TEER values from cell cultures according to equations 1-3.

$$R_{Mean\ cell\ culture} = \frac{R_{Cell\ culture} + R_{Cell\ culture} + R_{Cell\ culture}}{3} \tag{1}$$

$$R_{Mean\ blank\ membrane} = \frac{R_{Blank\ membrane} + R_{Blank\ membrane} + R_{Blank\ membrane}}{3} \tag{2}$$

$$R_{\text{True cell culture}} = R_{\text{Mean cell culture}} - R_{\text{Mean blank membrane}} \tag{3}$$

4.4   Cell staining

Following section will cover the staining procedure from cell fixation to different staining methods, description of antibodies evaluated, the set up of antibody combinations and data analysis of immunofluorescent samples collected through confocal microscopy to determine the protein expression.

4.4.1   Cell fixation

Cell cultures were fixated in 4% paraformaldehyde (PFA) (HistoLab, 02176) for 20 minutes. The removal of PFA was followed by washing with PBS (Gibco, 10010-015). Cell cultures were kept in PBS (Gibco, 10010-015) at 4°C until forthcoming analysis.

4.4.2   Embedding and sectioning

Membranes were cut loose using 6 mm biopsy punches (Integra Miltex, PA, USA). Membranes were dehydrated with the tissue processor Microm STP 120 (MICROM International GmbH, Walldorf, Germany) according to protocol, see Appendix B. Membranes were cut in half and embedded in paraffin. A Leica RM2165 mictrotome (Leica, Copenhagen, Denmark) was used to obtain 0.3 μm slices mounted on microscope slides.

4.4.3   Immunoperoxidase staining

Microscope slides containing cell culture sections were dewaxed and rehydrated in xylene and in graded ethanol solutions (99.5%, 95%, 70% and 50%). Detection of antigens were improved by incubation with Dako Target Retrieval Solution (Dako, S1699) at 96°C. Endogenous peroxides were blocked by incubation with 1% hydrogen peroxide (H_2O_2) (AppliChem, A0626,0250) in methanol. Avidin and biotin binding sites were blocked using Streptavidin/Biotin Blocking Kit (Vector Laboratories, SP-2002) and background staining was reduced by blocking unspecific bindings with block buffer; 1% BSA (Sigma, A9418), 5% Goat serum (Vector Laboratories, S-1000) and 0.05% Tween-20 (Sigma, P1379) in PBS (Gibco, 10010-015). Primary antibodies were diluted (1-2 μg/ml) in block buffer and incubated

for 1-2 hours at room temperature or over night at 4°C followed by incubation with biotinylated secondary antibody, 0.67 µg/ml diluted in block buffer, for 60 minutes. Biotinylated secondary antibodies were treated with avidin-biotin complex through R.T.U. Vectastain Elite ABC-Peroxidase Reagent (Vector Laboratories, PK-7100) and visualized through staining with ImmPACT NovaRED (Vector Laboratories, SK-4805). Counter staining was performed in hemotoxlin. Samples were dehydrated in graded ethanol (80%, 95% and 99.5%) and in xylene prior to permanent mounting in VectaMount Permanent Mounting Medium (Vector Laboratories, H-5000).

Negative controls were performed by incubation of IgG antibodies, see table 5, from the same host as the intended primary antibody and with the same concentration.

4.4.4 Immunofluorescent staining

Cell cultures were permeabilized with 0.25% Triton X-100 (Sigma, T-6878) in PBS (Gibco, 10010-015) for 20 minutes. Background staining was reduced by blocking unspecific bindings with block buffer; 2.5% BSA (Sigma, A9418), 5% Goat serum (Vector Laboratories, S-1000) and 0.05% Tween-20 (Sigma, P1379) in PBS (Gibco, 10010-015) for 30 minutes. Primary antibodies were diluted to 1 µg/ml in blocking buffer and incubated with cells for 60 minutes. Secondary fluorescent labelled antibodies were diluted to 0.5-1 µg/ml in PBS and incubated for 30 minutes. Cell cultures were permanently mounted onto microscope slides with Vectashield Mounting Medium with DAPI (Vector Laboratories, H-1200) and sealed with cover glass and nail polish. Samples were stored in -20°C until visualization.

In cases of signal enhancement, the previous description was slightly modified. Primary antibody incubation was followed with incubation of biotinylated IgG antibody, 0.67 µg/ml in block buffer. Visualization of the antibody was performed using a strepavidin conjugated fluorescent antibody, 0.5-1 µg/ml in PBS (Gibco, 10010-015).

Negative controls were performed by incubation of IgG antibodies, see table 5, from the same host as the intended primary antibody and with the same concentration.

4.4.5 Hematoxylin/Eosin staining

Microscope slides containing samples of cell culture sections were stained according to Mayers hematoxylin/Eosin protocol, see Appendix C, using an automatic slide stainer, Sakura DRS 601 Diversified Stainer (Sakura Finetek USA, Inc., Torrence, CA, USA).

4.4.6 Antibody evaluation

To visualize cell types and cell markers, antibodies were tested both through immunoperoxidase and immunofluorescent staining. Evaluated antibodies can be seen in table 2.

Table 2: Antibodies evaluated during the project for visualization of cell types and cell markers. Documented use of individual antibodies can be seen in the right column.

Antigen (Supplier)	Target	Host/Isotype	Clonality	Ref.
β-Tubulin (Abcam, ab6046)	Cilia	Rabbit IgG	Polyclonal	[76]
CCSP (Aviva, ARP41524)	Clara cells	Rabbit IgG	Polyclonal	
FoxJ1 (Antibodies, ABIN734288)	Ciliated cells	Rabbit IgG	Polyclonal	
FoxJ1 (eBioscience, 14-9965)	Ciliated cells	Mouse IgG1	Monoclonal	[77]
FoxJ1 (Sigma, HPA005714)	Ciliated cells	Rabbit IgG	Polyclonal	
KI-67 (Dako, M7240)	Proliferation	Mouse IgG1	Monoclonal	
MUC5AC (Abcam, ab3649)	Goblet cells	Mouse IgG1$_\kappa$	Monoclonal	[78, 79]
MUC5AC (Thermo, MS145-P1)	Goblet cells	Mouse IgG1$_\kappa$	Monoclonal	[80]
p63 (Abcam, ab53039)	Basal cells	Rabbit IgG	Polyclonal	
p63 (Atlas Antibodies, HPA006288)	Basal cells	Rabbit IgG	Polyclonal	
p63 (R&D Systems, MAB1916)	Basal cells	Mouse IgG2$_\beta$	Monoclonal	
p63 (Santa Cruz, sc-8343)	Basal cells	Rabbit IgG	Polyclonal	[81]
SP17 (Biorbyt, orb100865)	Cilia	Rabbit IgG	Polyclonal	
SP17 (Sigma, HPA037568)	Cilia	Rabbit IgG	Polyclonal	
TUBB4 (Abcam, ab119254)	Cilia	Mouse IgG2$_\beta$	Monoclonal	
TUBB4 (GeneTex, GTX102095)	Cilia	Rabbit IgG	Polyclonal	
TUBB4 (Novous, NBP2-00927)	Cilia	Mouse IgG2$_\beta$	Monoclonal	
TUBB4 (Thermo, PA5-21416)	Cilia	Rabbit IgG	Polyclonal	
ZO-1 (Abcam, ab59720)	Tight junctions	Rabbit IgG	Polyclonal	[78]
ZO-1 (BD, 610966)	Tight junctions	Mouse IgG1	Monoclonal	[82]
ZO-1 (Invitrogen, 33-9100)	Tight junctions	Mouse IgG1$_\kappa$	Monoclonal	[78]
ZO-1 (Invitrogen, 61-7300)	Tight junctions	Rabbit IgG	Polyclonal	[83]

Biotinylated antibodies used to visualization of immunoperoxidase stained samples and for signal enhancement of fluorescent stained samples can be seen in table 3.

Table 3: Biotinylated antibodies used to visualize primary antibodies through immunoperoxidase staining and as signal enhancement for fluorescent staining.

Reactivity	Target isotype	Host	Supplier
Mouse	IgG	Goat	Vector Laboratories (BA-1000)
Rabbit	IgG	Goat	Vector Laboratories (BA-9200)

Fluorescent labelled antibodies used to visualize immunofluorescent stained cell samples can be seen in table 4.

Table 4: Fluorescent labelled secondary antibodies, describing host specificity and target isotype. H+L isotype indicates reactivity to both IgG heavy chains and all light chains for the specific reactivity specie.

Reactivity	Target isotype	Host	Label/Dye	Supplier
Mouse	IgG (H+L)	Goat	Alexa Fluor 488	Invitrogen (A-11001)
Mouse	IgG2b	Goat	Alexa Fluor 488	Invitrogen (A-21141)
Mouse	IgG (H+L)	Goat	Alexa Fluor 568	Invitrogen (A-11004)
Mouse	IgG1	Goat	Alexa Fluor 568	Invitrogen (A-21124)
Rabbit	IgG (H+L)	Goat	Alexa Fluor 568	Invitrogen (A-11011)
Biotin (Streptavidin)	-	-	Alexa Fluor 488	Invitrogen (S-32354)

Antibodies used for negative controls can be seen in table 5.

Table 5: Antibodies used for negative control with peroxidase and immunofluorescent stained samples.

Reactivity	Target isotype	Supplier
Mouse	IgG	Vector Laboratories (I-2000)
Rabbit	IgG	Dako (X0936)

4.4.7   Antibody combinations - Scratch assay

The combinations and concentrations used for the scratch assay were determined from the previous described antibody evaluation and can be seen in table 6.

Table 6: Combinations of antibodies used in the scratch assay to perform double staining. The secondary antibodies are presented with concentration used in parenthesis.

Combination	Primary antibody	Primary antibody concentration	Secondary antibody
1	FOXJ1 (eBioscience)	3 μg/ml	568 Mouse IgG1 (1 μg/ml)
1	TUBB4 (Novus)	1 μg/ml	488 Mouse IgG2b (0.5 μg/ml)
2	MUC5AC (Thermo)	1 μg/ml	568 Mouse IgG1 (0.5 μg/ml)
2	TUBB4 (Novus)	1 μg/ml	488 Mouse IgG2b (0.5 μg/ml)
3	p63 (Atlas Antibodies)	3 μg/ml	488 Strep.av. (0.8 μg/ml)
3	KI-67 (Dako)	1 μg/ml	568 Mouse IgG (H+L) (1 μg/ml)
4	ZO-1 (BD)	1 μg/ml	488 Strep.av. (1 μg/ml)
4	p63 (Santa Cruz)	1 μg/ml	568 Rabbit IgG (1 μg/ml)

4.4.8 Image capture and analysis

Image analysis were performed on immunofluorescent stained cell cultures in the scratch assay using confocal microscopy to capture images of the different samples and staining. A Nikon Eclipse 90i (Nikon Corporation, Tokyo, Japan) confocal unit was used with supplied EZ-C1 software Gold version 3.50, build 724 (Nikon Corporation, Tokyo, Japan). Settings used for visualization of double staining were set according to table 7. Image capture was conducted using a plan apochromat 10.0x/0.45/4.00 dry objective and a plan apochromat 40.0x/0.95/0.14 correction ring spring-loaded, CGC 0.11-0.23 mm objective. The offset was set to 127, dwell time to 1.68 μs and a 30 μm pinhole was used.

Table 7: Setting used in the EZ-C1 software controlling the confocal unit. The four double staining combinations previous described were set using individual gains for each fluorophore. The coverage of the image area in relation to total membrane area is shown in parenthesis.

Combination	Gain 488	Gain 568	Zoom (Coverage)
1	99	73	10x (5%)
2	88	73	10x (5%)
3	100	83	10x (5%)
4	87	-	40x (0.3%)

Three images were collected for each sample. Image analysis was performed using

the image software ImageJ[3] with the extension[4] of "LOCI Tools" allowing ImageJ
to operate the Nikon .ids image file format. Each image was analysed by selecting
three regions of interest (ROI). These ROI's were placed at different areas, trying
to cover all aspects characterizing the image. The three specific ROI's were used
for analysing all images from all co-combinations, allowing analysis of 60% of the
image.

4.5 Gene expression

Following section describes the procedure used to investigate gene expressions
within the cell cultures, starting with cell preparation and purification of mRNA
to the different gene assays used and data analysis.

4.5.1 Lysis of cell cultures

Upon sample taking, cells were washed once in PBS (Gibco, 10010-015) and put on
wet ice. Cells were lysed in 200 µl 1:1 volume/volume Total RNA Lysis Solution
(Applied Biosystems, 4305895)/PBS (Gibco, 10010-015). The lysed cell samples
were transferred to Eppendorf tube on dry ice and stored in -80°C until RNA
purification.

4.5.2 RNA purification

Lysed cell samples were loaded on to a 96 well Total RNA Purification tray (Ap-
plied Biosystems, 4305673) fitted on a ABI Prism 6100 Nucleic Acid PrepStation
(Applied Biosystems, Foster City, CA, USA). RNA purification was performed ac-
cording to protocol from Applied Biosystem, see table D1 in Appendix D. Collected
samples were stored in 96 well plates in -80°C upon cDNA synthesis.

4.5.3 cDNA synthesis

Using a High Capacity cDNA Reverse Transcription Kit (Applied Biosystems,
4368813) according to protocol from Applied Biosystems, a 2x RT master mix was
prepared on ice. Containing 2.0 µl 10x RT Buffer (Applied Biosystems, 4319981),

---

[3]Schneider C.A., Rasband W.S. and Eliceiri K.W. NIH Image to ImageJ: 25 years of image
analysis. *Nature Methods*, 2012. 9(7):671-675.

[4]Found at Open Microscopy Environment web page; http://www.openmicroscopy.org/

0.8 µl 25x dNTP Mix (100mM) (Applied Biosystems, 362271), 2.0 µl 10x RT Random Primers (Applied Biosystems, 4319979), 1.0 µl MultiScribe Reverse Transcripase (Applied Biosystems, 4319983) and 4.2 µl nuclease-free water, for each reaction. For negative controls, MultiScribe Reverse Transcriptase was replaced with nuclease-free water.

RNA samples were transferred to a nuclease-free 96 well plate and mixed with equal amounts of 2x RT master mix to a final volume of 20 µl/reaction. The cDNA synthesis was performed using a PCR cycler, Veriti 96 well Thermal Cycler (Applied Biosystems, Foster City, CA, USA), programmed according to Applied Biosystems starting with incubation in 25°C for 10 minutes followed by 37°C for 120 minutes and 85°C for 5 minutes. cDNA samples were stored in -20°C until TaqMan experiments.

4.5.4   TaqMan assay

cDNA samples were diluted to 1-3 ng/ml. Assay mixes were prepared according to protocol from Applied Biosystems, see table D2 in Appendix D. Samples of 3 µl diluted cDNA and 7 µl assay mix were transferred to a MicroAmp Optical 384-Well Reaction Plate (Applied Biosystems, 4309849). Negative controls were mixed using 3 µl nuclease-free water and 7 µl assay mix. Plates were sealed with MicroAmp Optical Adhesive Film (Applied Biosystems, 4311971). Quantitative real-time PCRs were performed using ABI Prism 7900HT Sequence Detection System (Applied Biosystems, Foster City, CA, USA). Samples were analysed separately with its own baseline to ensure amplification of a specific product using ABI Prism 7900HT SDS software (Applied Biosystems, Foster City, CA, USA. A threshold cycle value (C_T-value) was calculated from the software comparing at what specific PCR cycle the reporter dye exceed a baseline set automatic by the software.

4.5.5   Gene expression assays

Gene assays used for analysis of gene expression for the scratch assay can be seen in table 8. The gene name is followed by a description of the target marker function.

Table 8: Gene assays used in the TaqMan analysis to analyse gene expression for the scratch assay.

Gene	Target	Supplier	Assay ID
36B4	Reference gene	In house gene	-
Beta-actin	Reference gene	Applied Biosystems	4352935
Cornifin A	Squamous metaplasia	Applied Biosystems	Hs00954595_s1
FOXJ1	Ciliated cells	Applied Biosystems	Hs00230964_m1
GAPDH	Reference gene	Applied Biosystems	402869
Involucrine	Squamous metaplasia	Applied Biosystems	Hs00846307_s1
KI-67	Cellular proliferation	Applied Biosystems	Hs01032443_m1
MMP-9	Cellular migration	Applied Biosystems	Hs00234579_m1
MUC5AC	Mucin, Goblet cells	Applied Biosystems	Hs01370716_m1
p63	Basal cells	Applied Biosystems	Hs00978343_m1
PCNA	Cellular proliferation	Applied Biosystems	Hs00427214_g1
SP17	Cilia	Applied Biosystems	Hs01011126_m1
TUBB4	Cilia	Applied Biosystems	Hs00760066_s1
ZO-1	Tight junctions	Applied Biosystems	Hs01551861_m1

Gene assays used for analysis of gene expressions for the smoke assay can be seen in table 9. The gene name is followed by a description of the target marker function.

Table 9: Gene assays used in the TaqMan analysis to analyse gene expression for the smoke assay.

Gene	Target	Supplier	Assay ID
36B4	Reference gene	In house gene	-
Beta-actin	Reference gene	Applied Biosystems	4352935
Caspase-3	Cell apoptosis	Applied Biosystems	Hs00234387_m1
CDH1	Cell-cell adhesion	Applied Biosystems	Hs01023894_m1
DDIT3	Stress response	Applied Biosystems	Hs01090850_m1
FOXJ1	Ciliated cells	Applied Biosystems	Hs00230964_m1
GAPDH	Reference gene	Applied Biosystems	402869
HSPA6	Stress response	Applied Biosystems	Hs00275682_s1
IL-8	Interleukin 8	Applied Biosystems	Hs00174103_m1
KI-67	Cellular proliferation	Applied Biosystems	Hs01032443_m1
MMP-9	Cellular migration	Applied Biosystems	Hs00234579_m1
MUC5AC	Mucin, Goblet cells	Applied Biosystems	Hs01370716_m1
p63	Basal cells	Applied Biosystems	Hs00978343_m1
TXNRD1	Stress response	Applied Biosystems	Hs00182418_m1
ZO-1	Tight junctions	Applied Biosystems	Hs01551861_m1

4.5.6   Data analysis

Acquired C_T-values were normalized by subtracting the C_T-value from a geometric mean of the three reference genes ($C_{T_{reference}}$) from the C_T-values from the gene of interest ($C_{T_{target}}$), see equation (4).

$$\Delta C_{T_{target}} = C_{T_{target}} - C_{T_{reference}} \tag{4}$$

To calculate the fold change, the C_T-value from a null value is subtracted from every C_T-value followed by insertion of the $\Delta\Delta C_T$-value in equation (6).

$$\Delta\Delta C_{T_{target}} = \Delta C_{T_{target}} - \Delta C_{T_{null\ sample}} \tag{5}$$

$$2^{-\Delta\Delta C_{T_{target}}} \tag{6}$$

From each technical triplicate an average fold change are calculated and plotted with errorbars shown through standard error of the mean (SEM), see equation (7).

$$SE_{\bar{x}} = \frac{s}{\sqrt{n}} \tag{7}$$

where:

s is the sample standard deviation
n is the number of samples

4.6 Cell-IQ

Cell behaviours and movements, visualization of wound closure and analysis were conducted using the Cell-IQ system (CM Technologies, Tampere, Finland). Transwell 24 well plates used during cell cultivation were filled with 700 μl ALI medium to all wells and samples were preferable placed in the middle of the plate to ensure as little evaporation of medium as possible during image capture. Following the plate preparation, the plate lid was changed to Cell-Secure lid (ChipMan, 44003) designed with inlet and outlet gas connectors. To the gas outlet Acrodisc CR 13mm syringe filter with PTFE membrane (PALL, 4423) was mounted to ensure sterility and the lid was sealed to the plate with non coloured adhesive tape. The plate was mounted into one of the two sliding plate holders inside the Cell-IQ incubator and connected the inlet to the gas supply. Using the supplied Cell-IQ Imagen software (CM Technologies, Tampere, Finland) image z-stack were set to 17.6 μm, image exposure to 5 ms and gas inlet to 6 ml/minute distributed in a repeated cycle with 15 minutes of gassing followed by 30 minutes with no gas. Image capture was set to continuous image recording and was let to record until manually stopped. Medium change was performed accordingly to any other cell culture and the image capture was temporarily paused. Imagining of wound healing was captured with a CFI Plan Fluorescence DL10x (Nikon Corporation, Tokyo, Japan) objective, with a grid of 3×3 images chosen in the middle of the well. To visualize the whole well a grid of 9×9 images could be used.

The image analysis, with supplied Cell-IQ Analyser (CM Technologies, Tampere, Finland), was performed by merging the grids into one single image. As the large images generates large amount of data to analyse, all images were compressed to 40% of its original size. By manually generate samples of images to the Cell-IQ Analyser software, libraries were build containing approximately 1600-3000 images displaying cell layers and the wound, simulated by the membrane. During analysis,

each image was compared to the library resulting in data displaying the amount of area covered with cells versus the area of the wound.
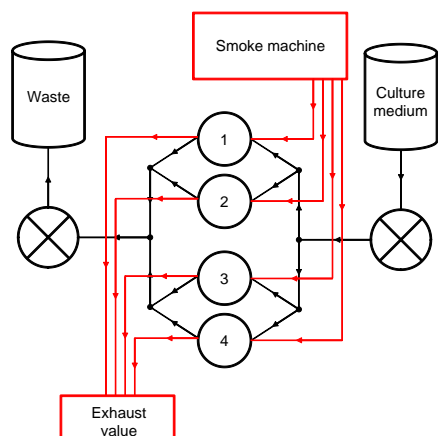
4.7   Smoke exposure

Cigarette smoke was generated through Borgwaldt RM20S® (Borgwaldt KC GmbH, Hamburg, Germany) smoking machine. According to protocol supplied by Borgwaldt, the Borgwaldt RM20S machine was let to warm up for 20 minutes followed by functional calibration. Calibration was conducted before every smoke experiments where the airflow through the machine was set to 20 cm/s and puff volume to 35 ml. Leakage test was conducted on all cigarette holders to ensure no leakage in the system. Whole cigarette smoke was generated from Kentucky Reference 2R4F cigarettes (University of Kentucky, Lexington, KY, USA). Diluted cigarette smoke was generated according to international smoking standards with a 35 ml smoke puff drawn over a time of two seconds every one minute. Transwell inserts containing differentiated NHBE cells were mounted into sterile whole smoke exposure chambers (British American Tobacco, patent publication No.WO 03/100417) under sterile conditions.

A modified model based on previous publication [71] was used, where the whole smoke exposure chambers were connected to the Borgwaldt RM20S smoking machine and a culture medium feeding system according to figure 6a. Peristaltic pumps were used to deliver fresh medium into the chambers and to remove old medium. Up to four chambers, each containing up to eight inserts in air liquid interface seen in figure 6b, were able to be smoked during one session. DMEM (Gibco, 41965-039) was used as culture medium and was continuously fed into the basolateral compartment to keep cell cultures in air liquid interface. Culture medium and chambers were held at 37°C during smoke exposure experiments.

Evaluation of cigarette smoke to NHBE cell cultures was conducted at four different smoke dilutions; 1:5, 1:10, 1:20 and 1:50 volume/volume smoke/air. Smoke experiments were conducted during 30 minutes with DMEM (Gibco, 41965-039) fed at 10 ml/minute and chamber.

The smoke assay were conducted by exposure of 1:50 volume/volume smoke/air dilution for 30 minutes, with DMEM (Gibco, 41965-039) feed at 10 ml/minute and chamber.

(a) Illustration of the smoke exposure set up. Numbered circles are used to donate the four different exposure chambers.
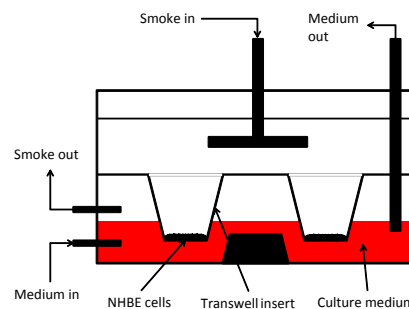
(b) Illustrative cross section of an exposure chamber describing the different flows and medium position to Transwell inserts. Medium and smoke are countercurrent feed in this model.

Figure 6: Schematic figures of the smoke exposure set up and the exposure chamber.

4.8   Compound treatment

AstraZeneca R&D in house compounds A, B and positive control C were used diluted in sterile DMSO (Sigma, D2438) in the three concentrations 0.1 µM, 1 µM and 10 µM. Differentiated NHBE cell cultures were treated, after scratch wounded according to previous described method, with 20 µl of compound applied apically.

5 Experimental plan

Following the method evaluation, experimental plans for the scratch assay and smoke assay were established. At a final stage of the project the scratch assay was used to perform one last experiment, the compound treatment, using three different AstraZeneca compounds to study their effect to wound healing.

5.0.1 Method evaluation

During the method evaluation different methods and techniques to introduce reproducible scratch wounds, using tools such as pipette tips and cell scrapers, were evaluated. Two different measuring devices for TEER measurements were evaluated on one cell donor.

Antibodies presented in table 2 were evaluated through two techniques; immunoperoxidase staining of sectionized NHBE cell cultures in order to distinguish the localization of binding sites and immunofluorescent staining on whole NHBE cell cultures to investigate potential use for image analysis. Potential double staining, using combinations of two different secondary antibodies, were evaluated through immunofluorescent staining on whole NHBE cell culture.

The Cell-IQ system was investigated to monitor and analyse cell migration and determine wound closure of scratch wounded cell cultures.

Four different cigarette smoke dilutions; 1:5, 1:10, 1:20 and 1:50 volume/volume smoke/air, were evaluated to NHBE cell cultures.

5.0.2 Scratch assay

The wound healing process of scratch wounded cell cultures were investigated mainly through four different read outs; formation of physiological barriers (TEER measurements), cell migration (Cell-IQ analysis), gene expression (TaqMan analysis) and protein expression (immunofluorescent staining). Samples were collected at eight different time points according to table 10. The assay was conducted three times, each time on a different donor. The three donors used are shown in table 1.

The TEER measurements were performed at the same culture inserts throughout the whole study, from day one in ALI until the end if the experiment. Cell-IQ analysis were conducted on scratch wounded cultures and monitored during one week. Investigated gene expressions by TaqMan analysis can be seen in table 8.

The protein expression was monitored through immunofluorescent staining according to previous described double staining, see table 6. For every double staining, negative control staining was conducted as previous described.

Table 10: Experimental plan describing the different analysis methods, time point and number of sample collected for the different analysis. Total number of samples for immunofluorescent staining are shown followed by the specific number of samples for the four different double staining. The experimental plan was conducted three times, each time on a different donor.

	Time point							
	-1 hr	0 hr	9 hr	14 hr	24 hr	33 hr	72 hr	2 w
Analysis method	**Number of samples**							
TEER	3							
Cell-IQ	1	3						
TaqMan	3	3	3	3	3	3	3	3
Immunofluorecent staining	12	12	12	12	12	12	12	12
· Basal cells · Tight junctions	3	3	3	3	3	3	3	3
· Basal cells · Proliferation	3	3	3	3	3	3	3	3
· Ciliated cells · Cilia	3	3	3	3	3	3	3	3
· Goblet cells · Cilia	3	3	3	3	3	3	3	3

5.0.3 Smoke assay

The effect of cigarette smoke on NHBE cell cultures was monitored through three major read outs; formation of physiological barriers (TEER measurements), cell migration (Cell-IQ analysis) and gene expression (TaqMan analysis). Samples were collected at six different time points according to table 11. The assay was performed once on one donor. Gene expressions were analysed through TaqMan where investigated genes can be seen in table 9.

The TEER measurements were conducted on cigarette smoke exposure samples at each time point prior to cell lysis for gene expression analysis. TEER measurements were conducted at the same time point on negative controls throughout the

experiment. Cell-IQ analysis was performed on three scratch wounded samples exposed to cigarette smoke and on three scratch wounded negative controls, not exposed to cigarette smoke.

Table 11: Experimental plan describing the different analysis methods, time point and number of samples collected for the different analysis.

	Time point					
	-1 hr	4 hr	8 hr	24 hr	48 hr	72 hr
Analysis method	**Number of samples**					
TEER	3	3				
Cell-IQ	3	3				
TaqMan	9	9	9	9	9	9

TaqMan samples were divided into three groups; smoked samples, smoke wounded samples and controls. The smoked samples were exposed to cigarette smoke, smoke wounded samples were prior to cigarette smoke exposure introduced to scratch wounds according to previous described method, and controls were not introduced to scratch wound nor cigarette smoke. Samples were divided according to table 12.

Table 12: TaqMan samples for the three different treatments used in the smoke exposure gene expression analysis.

	Time point					
	-1 hr	4 hr	8 hr	24 hr	48 hr	72 hr
Treatment	**Number of samples**					
Smoke	3	3	3	3	3	3
Smoke and wound	3	3	3	3	3	3
Control	3	3	3	3	3	3

5.0.4 Compound treatment

The effect of three different compounds were evaluated to scratch wounded cultures, performed according to previous described method. Diluted compounds A, B and C were applied on the apical side of cell cultures, according to table

13. Analysis was performed on cell migration and wound closure (Cell-IQ analysis). Negative controls were collected in triplicates for; scratch wounded cultures exposed to DMSO (Sigma, D2438) to investigate the DMSO effect to wound healing and non-treated scratch wounded cultures to compare to the DMSO treated samples.

Table 13: Experimental plan of the compound treatment. Due to shortage of time the experiment had to be performed with one sample per compound and concentration.

	Concentration		
	0.1 µM	1 µM	10 µM
Treatment	**Number of samples**		
Compound A	1	1	1
Compound B	1	1	1
Compound C	1	1	1

6 Results

The project was, as previous described, divided into four different parts; method evaluation, scratch assay, smoke assay and compound treatment. The results are presented, divided into the four parts, in following section.

6.1 Method evaluation

The methods used in the scratch assay and smoke assay were evaluated and tested in order to reproduce the experiment throughout the different parts of the project. Result from the evaluation influencing the oncoming project parts are visualized in the following section.

6.1.1 Scratch wounds

Through investigation of different tools to produce scratch wounds in the cell cultures, it was concluded that small hand-held tools were easier handled and controlled. By using plastic pipette tips in different sizes (100 µl, 300 µl and 1000 µl), it was seen that scratch wounds were lined by bankings of cells along the wound edge, see figure 7a. More over, the pipette tips produced an irregular wound shape hard to reproduce.

Using glass Pasteur pipettes did, in comparison to plastic pipette tips, not cause any bankings of cells along the wound edge and resulted in a sharp clean cut with a more constant wound shape with a fixed width, see fig 7b. Connecting the Paster pipette to a vacuum suction pump and applying a constant vacuum during the scratching, the removal of cells from the membrane were enhanced and aggregation of cells at the end of the scratch wound were reduced.
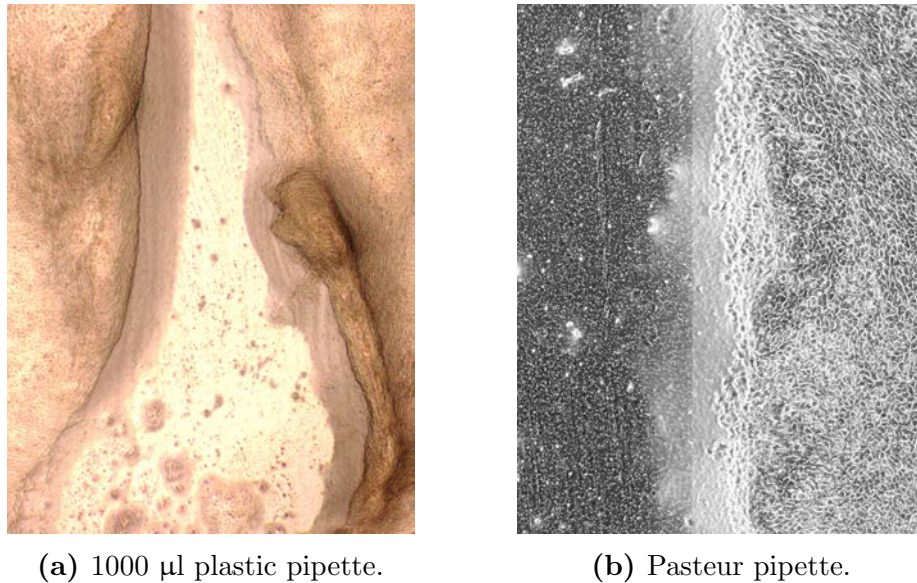
(a) 1000 µl plastic pipette.   **(b)** Pasteur pipette.

Figure 7: Evaluation of scratch wounds by two types of pipettes.

Scratches produced by Pasteur pipettes were measured through image analysis and were concluded to have an average width of 1.4 mm. Membrane area cleared of cells from this scratch technique was estimated through calculations and measurements to be 27% of the total culture area, see figure 8.
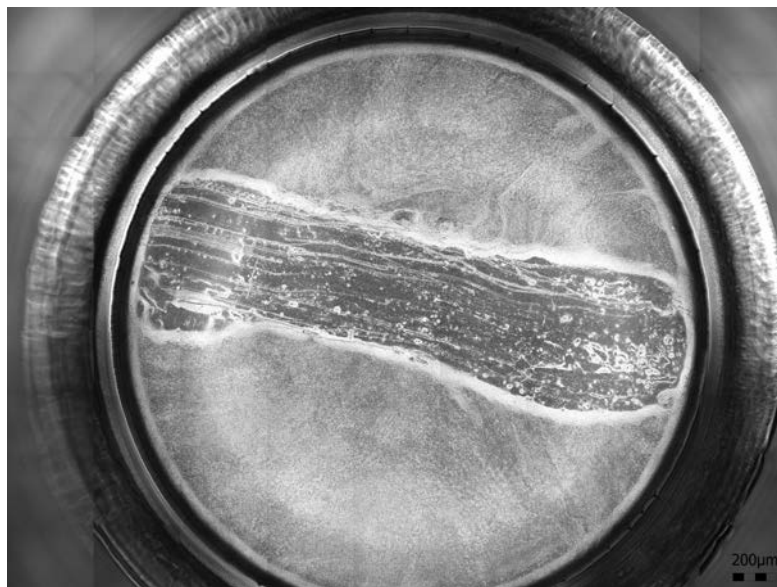
Figure 8: Scratch wounded cell culture.

Studying scratch wounds produced by Pasteur pipettes in microscope revealed damage to the membrane below the cell cultures. The depth and width of a membrane scratch was investigated by sectioning the membrane perpendicular to the scratch. Sections were visualized and investigated in bright field microscope, showing a destruction in the membrane, see figure 9.
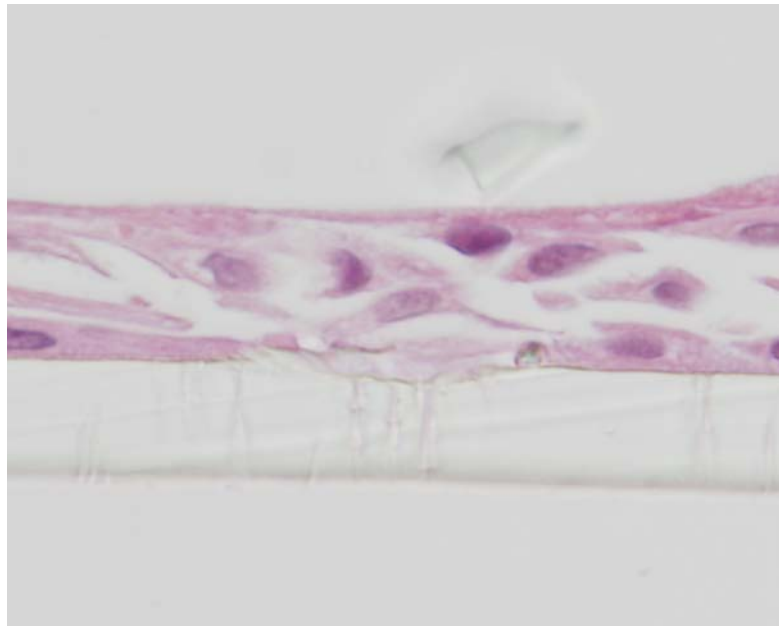
Figure 9: Section visualizing damage to the membrane caused by a Pasteur pipette during scratching.

6.1.2 Antibody evaluation

The antibody evaluation was as previously described divided into two parts. The initial part demonstrating the localisation of antibody binding to the NHBE cell culture by immunoperoxidase staining of culture sections. The later part demonstrate immunofluorescent staining of whole NHBE cell cultures.

The immunoperoxidase staining with antibodies specific to NHBE cell cultures can be seen in figure 10. Positive staining are shown in red while the counter staining are visualized in light blue representing non-stained areas.

The three major cell types, ciliated cells, goblet cells and basal cells were visualized through enzymatic staining as seen in figure 10. Ciliated cells were visualized by staining of FOXJ1 (eBioscience), see figure 10a. Red staining can be seen located in the nucleus of cells expressing cilia on the apical side. Staining of the cilia

was conducted through TUBB4 (Novus) seen as red staining located in the cilia in figure 10b. Staining with SP17 (Sigma) revealed staining in cilia as well as in the cytoplasm of ciliated cells, seen in figure 10c. The goblet cells were visualized through staining of mucin protein MUC5AC (Thermo), showing staining in spots in the apical part of the cells, representing the mucus granules, see figure 10d. Basal cells, visualized through staining of p63 (Atlas Antibodies) are seen in figure 10e, where they can be seen by nuclear staining of cells lining the membrane. Staining for Clara cells, through CCSP (Aviva), did not show any signal. To assure the specificity of the CCSP antibody, staining performed on human alveolar tissue showed a distinct signal, see figure 10f.

(a) FOXJ1 (eBioscience) **(b)** TUBB4 (Novus) **(c)** SP17 (Sigma)

(d) MUC5AC (Thermo) **(e)** p63 (Atlas Antibodies) **(f)** CCSP (Aviva)
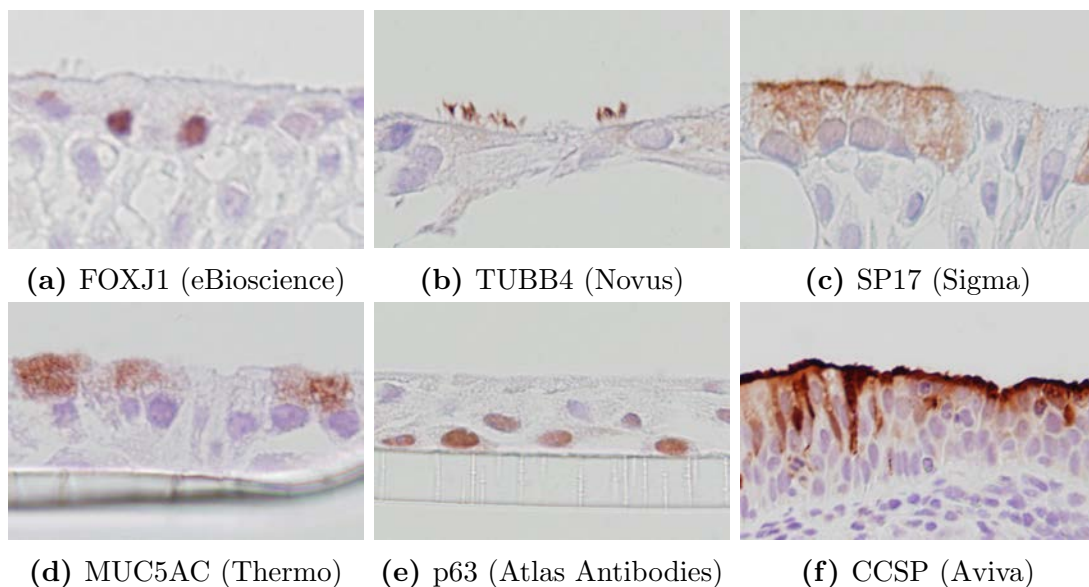
Figure 10: Staining of the major human airway epithelial cell types; ciliated cells (FOXJ1, TUBB4 and SP17), goblet cells (MUC5AC), basal cells (p63) and Clara cells (CCSP).

Specific cell markers for tight junctions and proliferative cells were visualized through immunoperoxidase staining, see figure 11. Tight junctions, visualized through staining of tight junction protein ZO-1 (BD), are shown by red dots at the apical size of the cell culture, see figure 11a. Proliferative cells were visualized by staining of KI-67 (Dako) shown through nuclear staining in figure 11b.

(a) ZO-1 (BD)   **(b)** KI-67 (Dako)
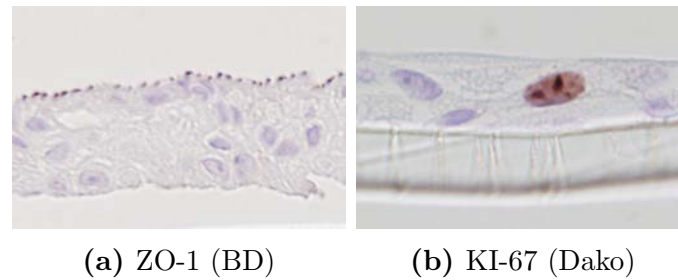
Figure 11: Staining of tight junctions (ZO-1) and proliferative cells (KI-67).

The result from the antibody evaluation through immunoperoxidase staining can be seen in table 14. Antibodies resulting in insufficient staining, either by non-specific staining or no staining, were not further used in the project.

Table 14: Results from antibodies evaluated through immunoperoxidase staining.

Antigen (Supplier)	Target	Comment to staining
β-Tubulin (Abcam, ab6046)	Cilia	Non-specific staining (whole cell)
CCSP (Aviva, ARP41524)	Clara cells	No signal in NHBE cell cultures
FoxJ1 (Antibodies, ABIN734288)	Ciliated cells	No signal
FoxJ1 (eBioscience, 14-9965)	Ciliated cells	See figure 10a
FoxJ1 (Sigma, HPA005714)	Ciliated cells	Non-specific staining (whole cell)
KI-67 (Dako, M7240)	Proliferation	See figure 11b
MUC5AC (Abcam, ab3649)	Goblet cells	Staining comparable to figure 10d
MUC5AC (Thermo, MS145-P1)	Goblet cells	See figure 10d
p63 (Abcam, ab53039)	Basal cells	Non-specific staining (basal cells and cilia)
p63 (Atlas Antibodies, HPA006288)	Basal cells	See figure 10e
p63 (R&D Systems, MAB1916)	Basal cells	No signal
p63 (Santa Cruz, sc-8343)	Basal cells	Staining comparable to figure 10e
SP17 (Biorbyt, orb100865)	Cilia	Non-specific staining (whole cell)
SP17 (Sigma, HPA037568)	Cilia	See figure 10c
TUBB4 (Abcam, ab119254)	Cilia	No signal
TUBB4 (GeneTex, GTX102095)	Cilia	No signal
TUBB4 (Novous, NBP2-00927)	Cilia	See figure 10b
TUBB4 (Thermo, PA5-21416)	Cilia	No signal
ZO-1 (Abcam, ab59720)	Tight junctions	No signal
ZO-1 (BD, 610966)	Tight junctions	See figure 11a
ZO-1 (Invitrogen, 33-9100)	Tight junctions	No signal
ZO-1 (Invitrogen, 61-7300)	Tight junctions	No signal

Antibodies specific to desired cell type or cell marker were investigated by im-

munofluorescent staining of whole cell cultures. Immunofluorescent staining of ciliated cells can be seen in figure 12a, where nuclear staining through FOXJ1 (eBioscience) are seen in red and cilia through TUBB4 (Novus) in green. Structural visualization of cilia can be seen at 60 times magnification in figure 12b. Visualization of cilia could also be seen by SP17 (Sigma), see figure E1 in Appendix E.
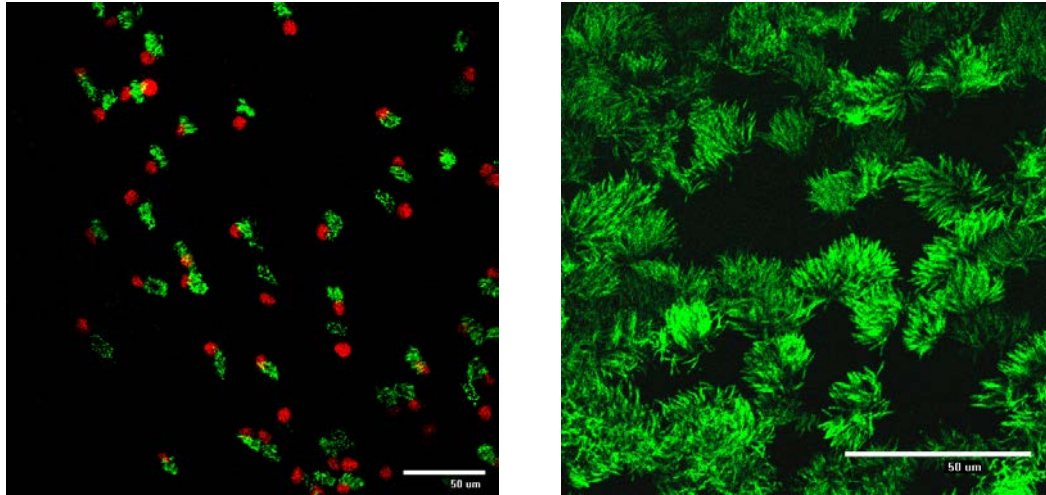
(a) FOXJ1 (red) and TUBB4 (green)   **(b)** TUBB4

Figure 12: Immunofluorescent staining of ciliated cells through nuclear staining by FOXJ1 and staining of tubulin in cilia by TUBB4.

Basal cells were stained through p63 (Atlas Antibodies) to cultures fixated at day 7 and day 39. Positive stained basal cells are seen in samples from day 7 compared to day 39 in figure 13, where basal cells are seen in pink and all cell nucleus are seen in blue through DAPI staining. Sample from day 7 were seen having a larger amount of positive stained cells compared to day 39. Basal cells were also seen using p63 (Santa Cruz), see figure E2 in Appendix E.

(a) Day 7 in ALI   **(b)** Day 39 in ALI
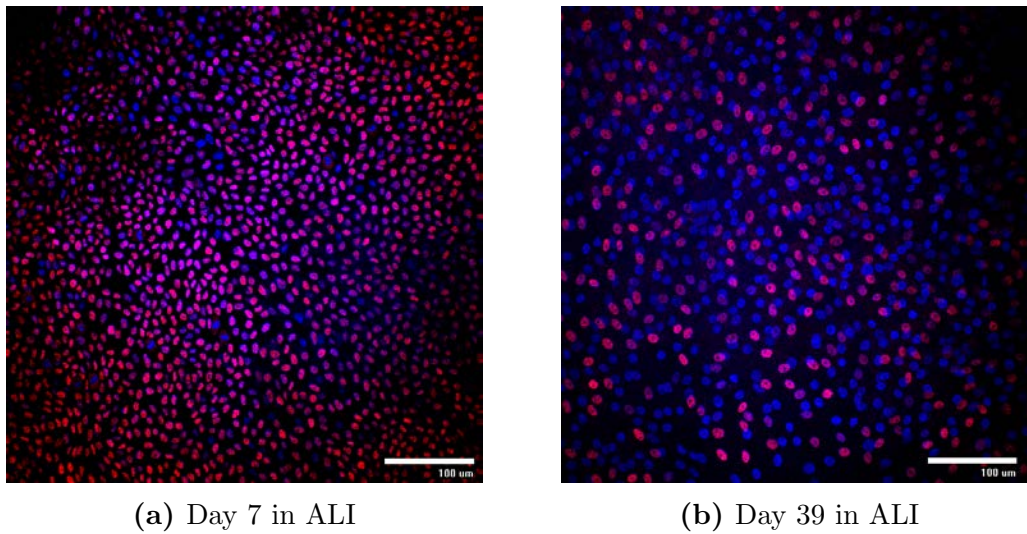
Figure 13: Immunofluorescent staining of basal cells through p63 (pink) together with DAPI (blue) for visualization of cell nucleus.

Visualization of tight junction protein ZO-1 (BD) was possible to distinguish from the background staining, using a biotinylated enhancement step, as a green mesh pattern seen in figure 14a together with cell nucleus seen in blue through DAPI staining. The formation of tight junction protein ZO-1 from culture cultivated for 7 days in ALI can be seen in figure 14b, where only sporadic meshed pattern could be found.

(a) ZO-1, day 30   **(b)** ZO-1 day 7
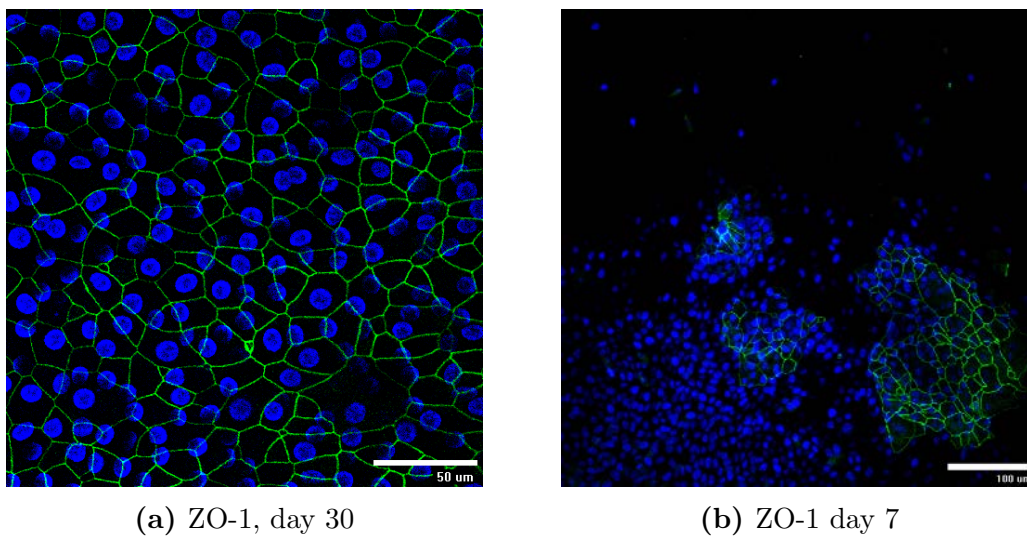
Figure 14: Immunofluorescent staining of tight junction protein ZO-1 (green) together with DAPI (blue) for visualization of cell nucleus.

Goblet cells were stained through MUC5AC (Thermo), seen in green in figure 15a. Visualization of proliferative cells through KI-67 (Dako) can be seen in red in figure 15b together with basal cells, through p63 (Atlas Antibodies), in green. Cells shown in orange or yellow were both positively stained with p63 and KI-67.

(a) MUC5AC   **(b)** KI-67 (red/yellow) and p63 (green)
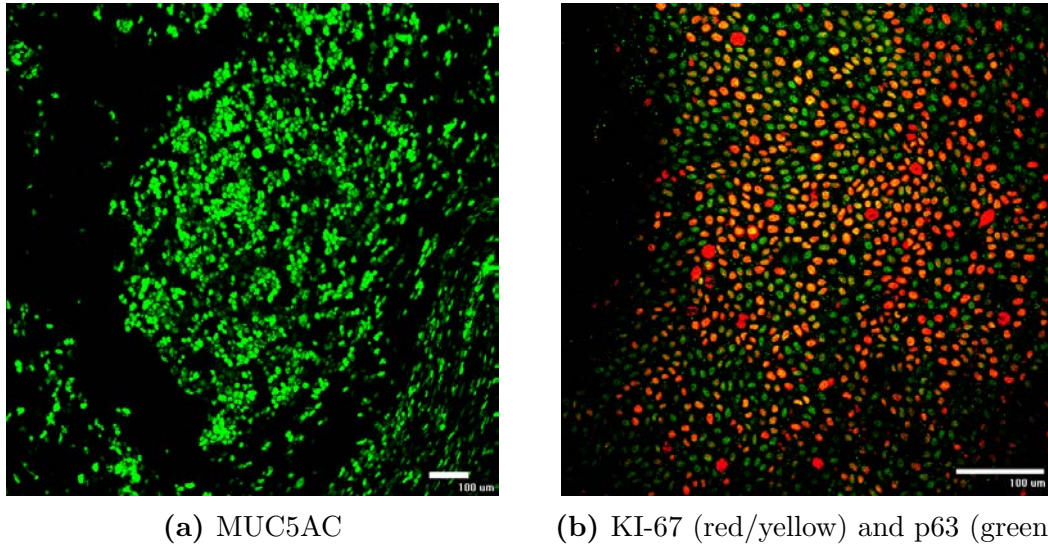
Figure 15: Immunofluorescent staining of goblet cells (MUC5AC), proliferative cells (KI-67) and basal cells (p63).

Different double staining combinations were discovered where two different markers could be used to analyse one cell population. Possible combinations of double stainings investigated can be seen in table 15.

Table 15: Possible double staining investigated.

Target	Primary Antibody	Primary Antibody
Mucins and cilia	MUC5AC (Thermo)	TUBB4 (Novus)
Mucins and cilia	MUC5AC (Thermo)	SP17 (Sigma)
Cilia and ciliated cells	TUBB4 (Novus)	FOXJ1 (eBioscience)
Basal cells and proliferative cells	p63 (Atlas Antibodies)	KI-67 (Dako)
Basal cells and tight junctions	p63 (Santa Cruz)	ZO-1 (BD)

6.1.3 Trans Epithelial Electrical Resistance

Evaluation of two different measuring devices, chop sticks and EndOhm, were performed during the scratch assay for donor 1849. The differences between the two devices are seen in figure 16, showing no significant difference between the two devices.
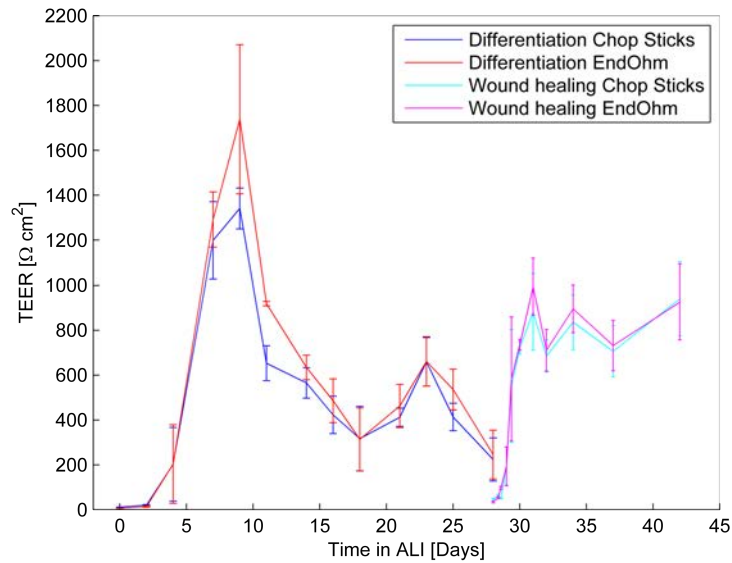
Figure 16: Evaluation of the two measuring devices, STX2 Chopsticks and Endohm, during differentiation and wound healing of donor 1849.

6.1.4 Cell-IQ

Using the Cell-IQ system over time did not seem to induce changes to the cell cultures, as the mucus production and TEER were compared similar to controls. Using continuous imaging, movements were seen within the cell culture and the migration could be analysed.

Images obtained during cell migration of scratch wounded cell cultures were analysed with the Cell-IQ analyser software. The analysis can be seen in figure 17 where a red mask was applied to the cell layer of each image. Figure 17 demonstrate three analysed images, at time point 0 hours post scratch wound, 28 hours post scratch wound where the cells had begun covering the nude membrane and 43 hours post scratch wound where the cell culture was fully healed.

(a) t=0h   **(b)** t=28h   **(c)** t=43h

(d) t=0h   **(e)** t=28h   **(f)** t=43h
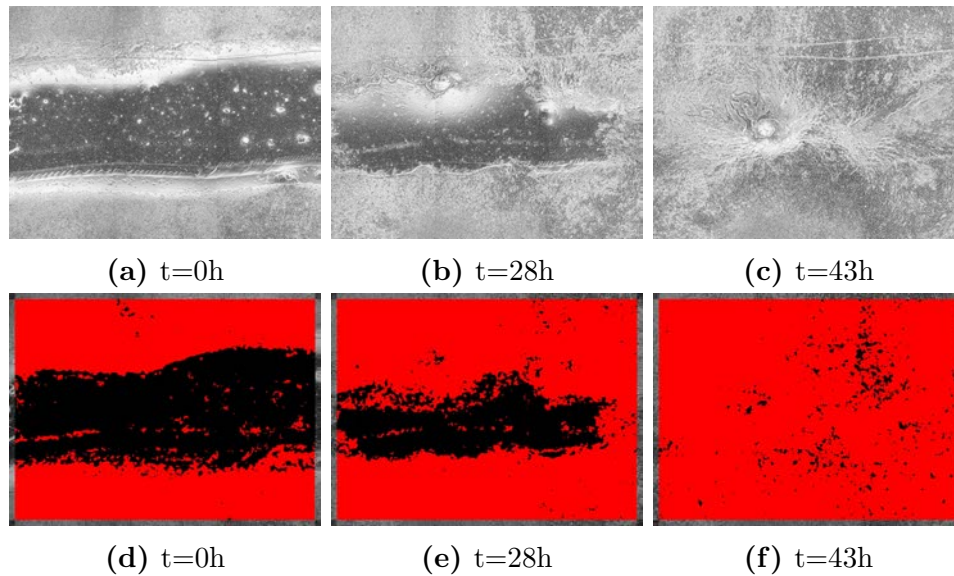
Figure 17: Top row (figures a, b and c) represent three images captured during wound healing. Bottom row (figures d, e and f) represent the analysis performed by Cell-IQ analyser, where a red mask was applied to the images to measure the cell migration. The three donated time point represent fresh scratch wound (t=0h), cells migrating into the wound (t=28h) and healed wound (t=43h).

Images captured of non-wounded cell culture did show an intense cell migration. A new type of image analysis[5] demonstrated the possibility to visualize this migration from one single image, as figure 18a, into a heat map structure, as seen in figure 18b, or into a vector field, as seen in figure 18c, where red parts are donated for areas with high migration and blue or black parts to low or absent migration.

(a) Whole culture   **(b)** Heat map   **(c)** Vector field
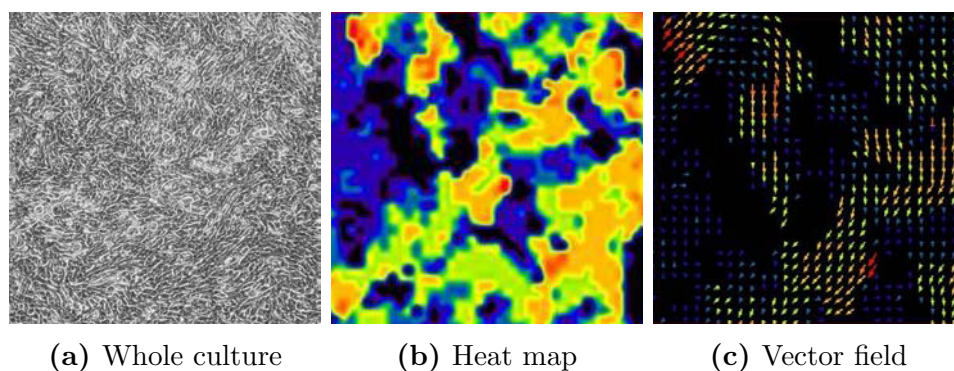
Figure 18: Analysis of non-wounded cell culture through heat map and vector field, enabling migration analysis of individual areas within a cell culture.

---

[5]Performed by Alan Sabirsh, Image expert, CVMD, AstraZeneca R&D Mölndal

6.1.5   Smoke exposure

Response of four different smoke dilutions were investigated in NHBE cell cultures. Dilutions of 1:20 and 1:50 volume/volume smoke/air did not show any significant loss of cell mass 24 hours post smoke exposure, or at any later stage in the evaluation. There were no visual differences between the 1:20 and 1:50 dilutions. Dilutions of 1:5 and 1:10 volume/volume smoke/air showed a major loss of cells 24 hours post smoke exposure following washing with PBS. Cell culture exposed to 1:10 smoke dilution seemed to recover over time where a confluent cell layer was seen once again after five days. The culture exposed to 1:5 smoke dilution showed only small sporadic clusters of cells five days post smoke exposure.

(a) 1:5, 24hr   **(b)** 1:10, 24hr   **(c)** 1:20, 24hr

(d) 1:50, 24hr   **(e)** 1:5, 5 days   **(f)** 1:10, 5 days
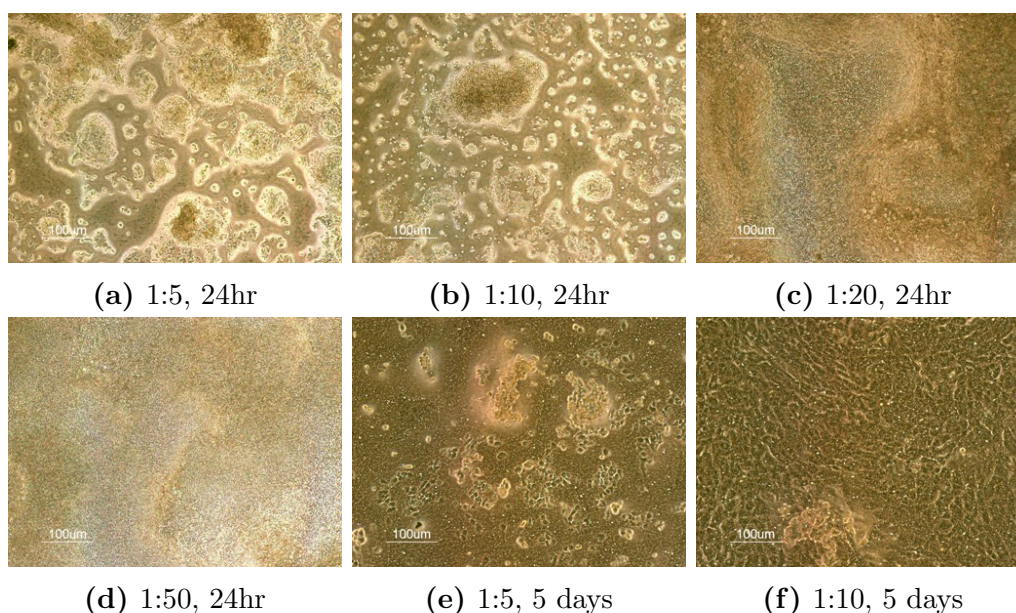
Figure 19: Evaluation of four different smoke exposure concentrations; 1:5, 1:10, 1:20 and 1:50 volume/volume smoke/air. No visual effects were observed for 1:20 and 1:50 dilutions. Dilutions of 1:5 and 1:10 showed a loss of cell mass 24 hours post exposure, were culture exposed to 1:10 dilution recovered after five days whereas culture exposed to 1:5 dilution had not recovered after five days.

6.2   Scratch assay

The results from the scratch assay are presented in the following section.

6.2.1 Cell culturing

During the cultivation of donor 1849 the incubator holding the cell cultures were used by a number of other researchers which resulted in a frequent opening and closing of the door. As a result of the frequent change in temperature, humidity and CO_2 the cell cultures stopped to, visually, produce mucus and the TEER value dropped below 400 $\Omega \cdot cm^2$ at two time points, as seen in figure 20.

All three donors showed production of mucus to the naked eye around day 15 and ciliated cells were seen around day 21. A visible difference in mucus production between the three donors during cultivation was identified as donor 1849 had larger mucus production compared to the other two donors. The mucus produced by donor 1849 was less sticky and more watery. Donor 4449 had greater variation in mucus production, starting with watery and non sticky mucus which by time became more sticky and harder to remove. Donor 12240 produced rather early a thin layer of mucus which was difficult to remove by vacuum suction or washing.

6.2.2 Physiological barriers

Investigation of the formation of physiological barriers through TEER measurements during the differentiation phase for the three cell donors can be seen in figure 20. During evaluation of donor 1849 and donor 12240 the resistance was seen to rapidly increased at day 4 to a value above 1000 $\Omega \cdot cm^2$, while donor 4449 showed a slower increase in resistance and reached same TEER value at day 10. When fully matured the cell cultures showed a TEER value between 500-1000 $\Omega \cdot cm^2$, which was seen by all three donors. As a result of heavy work load on the incubator during cultivation of donor 1849, the TEER values dropped blow 400 $\Omega \cdot cm^2$ at several time points during the differentiation phase as previous mentioned.
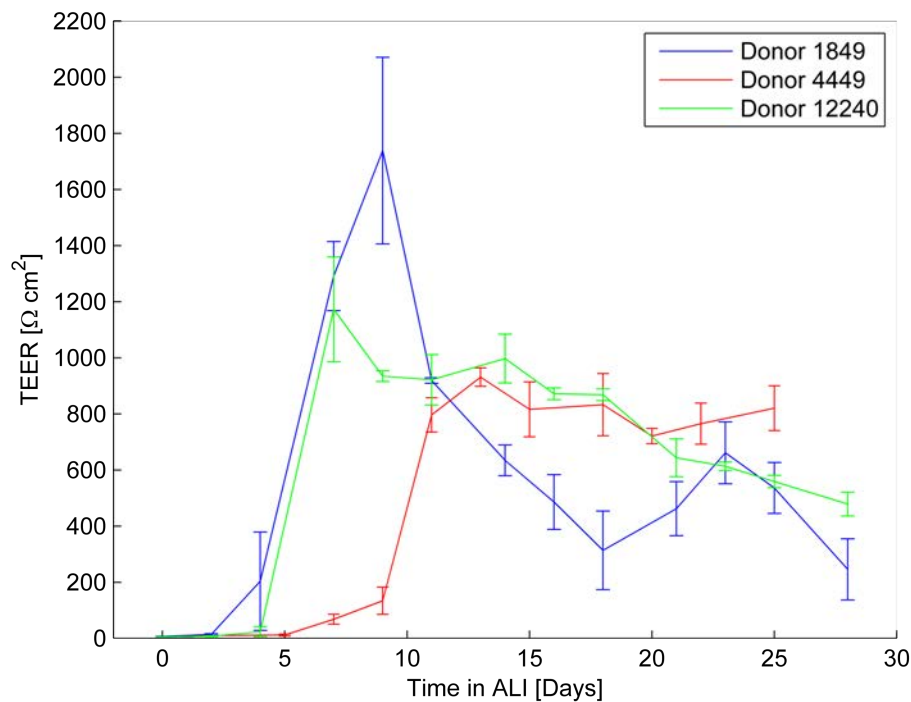
Figure 20: Electrical resistance during cell differentiation followed through TEER measurments. Three different donors, each represented by three cultures, were investigated. TEER values were collected in triplicates for each culture investigated.

As a result of introducing scratch wounds to the cell cultures, the TEER values instantly dropped to approximately 35-40 $\Omega \cdot cm^2$. The recovery phase from the scratch wound can be seen in figure 21, where the stars indicates the time where the scratch wound were visually closed. As seen, the TEER values were low when scratch wounds were visually closed and continued to increase. After approximately 100 hours, the TEER values were stabilized, measuring over 400 $\Omega \cdot cm^2$ for all three donors.
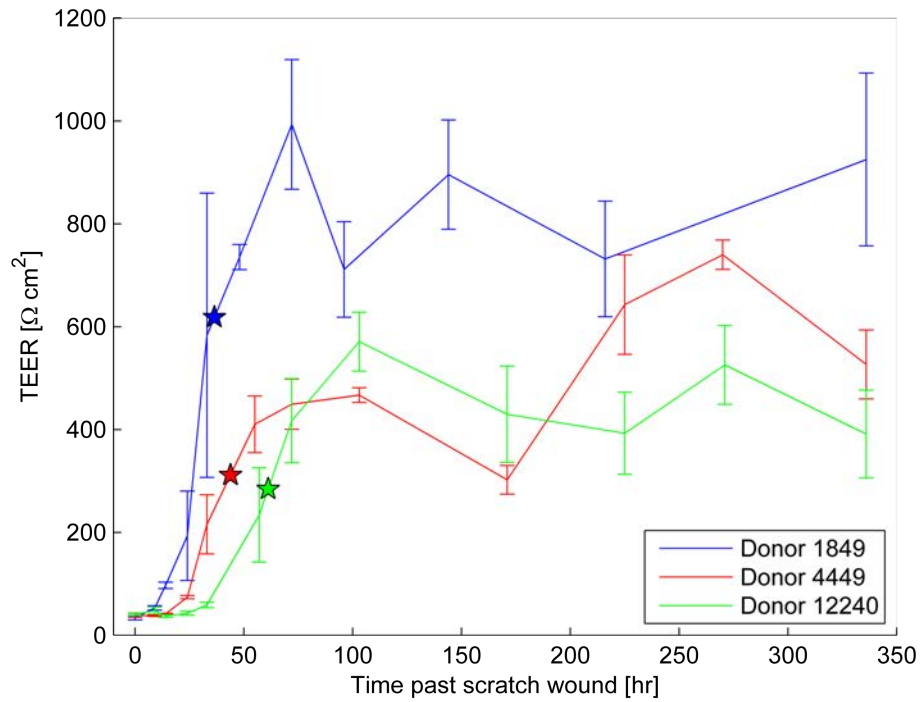
Figure 21: Electrical resistance during healing of scratch wounds. Stars representing visual closure of scratch wounds.

Investigating the gene expression of tight junction protein ZO-1, no obvious change during the wound healing was seen, see figure 22a. Images captured of ZO-1 immunofluorescent stained samples were difficult to analyse since the protein was located within a thin part of the apical layer. Image analysis of these images were hard to perform and were considered to be too time consuming and therefore determined not to be done. It was seen that the formation of ZO-1 adjacent to the wound edge were comparable to non-wounded cultures, compare figures 14a and 22b.
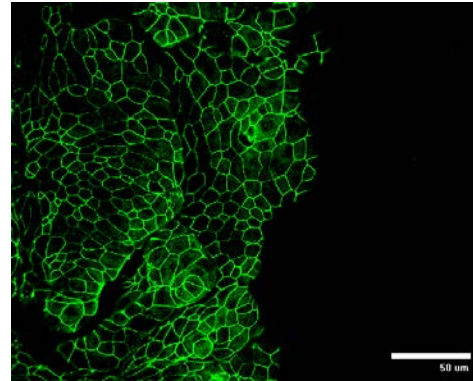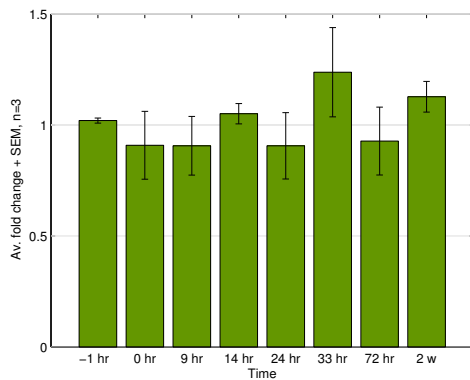
(a) Gene expression of tight junction protein ZO-1.

(b) Immunofluorescent image showing ZO-1 adjacent to the wound (right side black part), magnification 40x.

Figure 22: Analysis of gene expression and protein expression of tight junction protein ZO-1.

6.2.3   Cell migration

Images captured through the Cell-IQ's Imagen software were analysed by presenting guide image libraries, individual for each donor and composed of approximately 3000 images each. The migration was analysed by following the cell sheet propagation over the nude membrane over time, showed in figure 23. The image represent the migration for the three donors, where the dark coloured lines represent the mean migration while the light coloured areas displays floating error bars. The dotted line seen by donor 12240 starting at 70 hours represents two of the three samples monitored, as the Cell-IQ's image capture software crashed during imaging capture. As seen in figure 23, donor 1849 had the highest migration speed followed by donor 4449 and last donor 12240. Similar migration speed could be seen between donor 1849 and donor 4449, where donor 4449 showed a lag phase during the first 15 hours before migration start. Donor 12240 and donor 1849 seemed to start migrating direct after the scratch wound was introduced, where donor 12240 have a constant low migration speed. Triangles in the figure represents the closure of each individual sample and the stars the mean closure time for each donor.
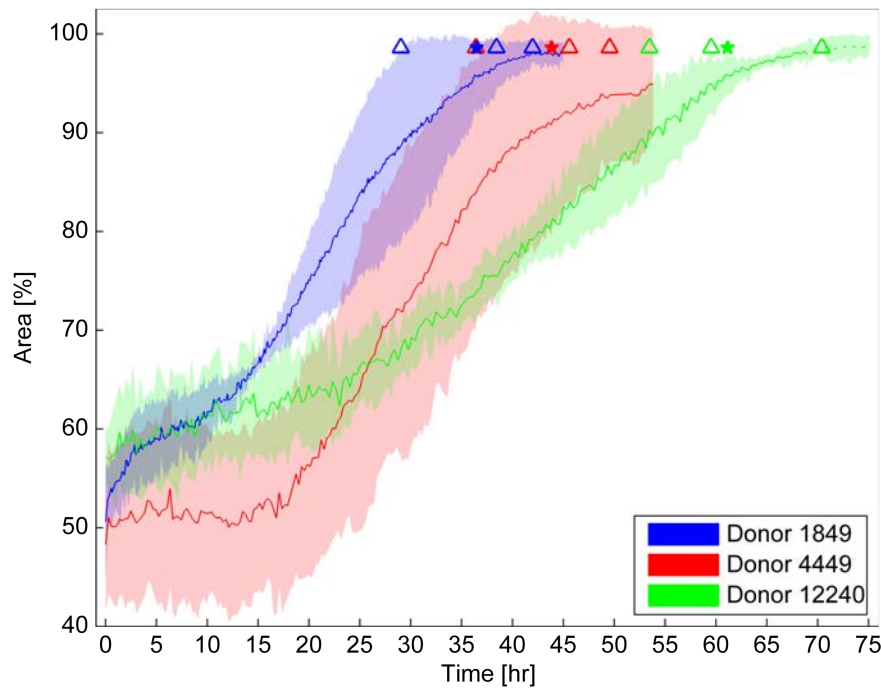
Figure 23: Cell migration over denuded membrane simulating wound healing. As the graphs reaches 100% area, the cell cultures are fully healed and cells covers the membranes as it was prior to the scratch wound.

Average wound closure time determined through visual investigation and the average closing area, determined by the Cell-IQ, can be seen in table 16.

Table 16: Average closure time, visual determined, for wound closure followed by its standard deviation and the average closure area.

Donor	Average closure time	Std.	Average closure area
1849	36h 28min	6h 41min	97.3%
4449	43h 50min	6h 44min	92.7%
12240	61h 7min	5h 35min	96.7%

The cell migration was also analysed through the gene expression of MMP-9. An up regulation of MMP-9 was seen over time, with a clear variation within the samples as seen in figure 24.
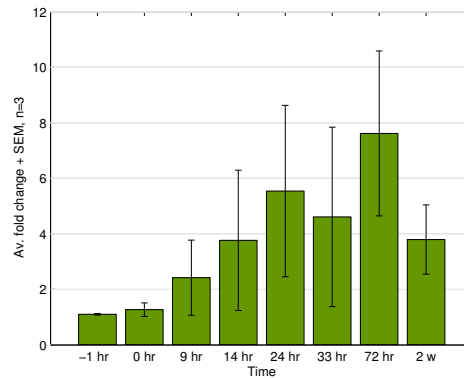
Figure 24: Gene expression of MMP-9, a matrix metalloproteinase linked to cellular migration in bronchial epithelial cells, during wound healing represented by the three donors.

In connection to the migration, gene expression of squamous markers were investigated through squamous metaplasia marker cornifin A and involucrine. An up regulation of cornifin A between 0 hours and 14 hours was seen followed by a drop in expression back to normal levels. Involucrine had a similar pattern the 14 first hours, but the later time points showed large variance, as seen in figure 25.
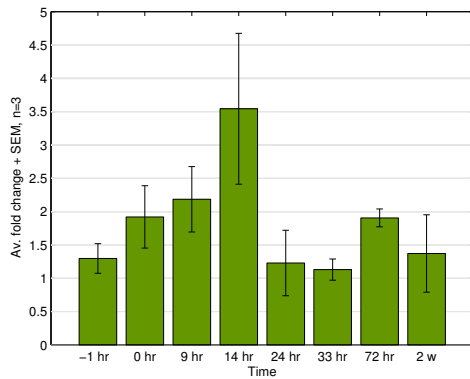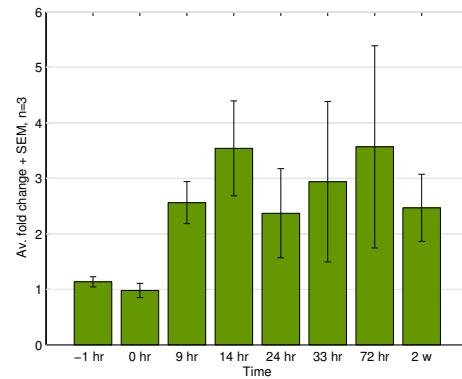
(a) Cornifin A   **(b)** Involucrine

Figure 25: Gene expression of squamous metaplasia markers during wound healing, represented by the three donors.

6.2.4   Cell proliferation

The proliferation within the cell cultures were investigated through gene and protein expression of proliferation marker KI-67. Analysing the gene expression data, the proliferation showed constant expression until 24 hours, where an up regulation could be seen with an increase in expression 33 hours and 72 hours post scratch wound. After 2 weeks, the expression levels were back to normal again, see figure 26a. Protein expression of KI-67 did in contrast to gene expression not show any clear tendency except a decrease at 2 weeks, see figure 26b.
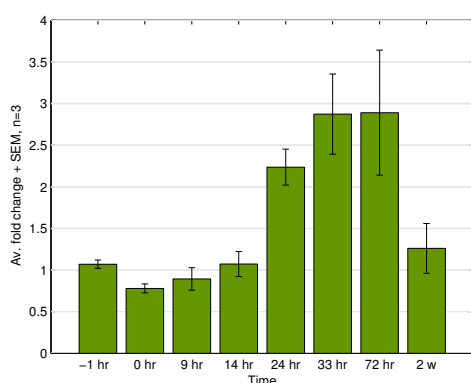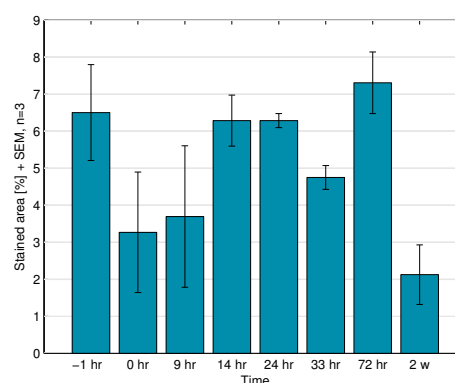
(a) Gene expression of KI-67.   **(b)** Protein expression of KI-67.

Figure 26: Analysis of gene and protein expression of proliferation marker KI-67. Gene expression is visualized through average fold change while protein expression is visualized by image analysis of percent stained area. The graphs are represented by the three different donors.

Compared to KI-67, another proliferation protein, PCNA, did not show any major change in gene expression over time, see figure 27.
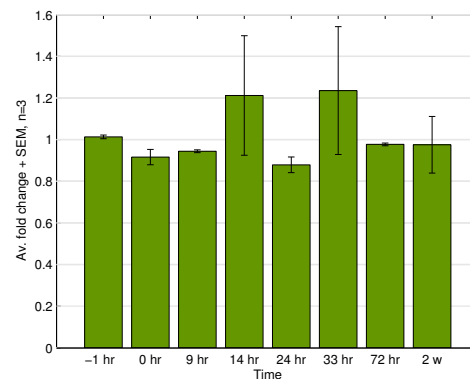
Figure 27: Gene expression of proliferation marker PCNA during wound healing, represented by the three donors.

6.2.5   Cell populations

Analysis of the three major cell populations; basal cells, ciliated cells and goblet cells were performed both through gene expression and protein expression.

Gene expression of basal cell marker p63 was up regulated over time, see figure 28a. Protein expression investigated through image analysis showed, on the contrary to gene expression, a down regulation in p63 over time, see figure 28b.
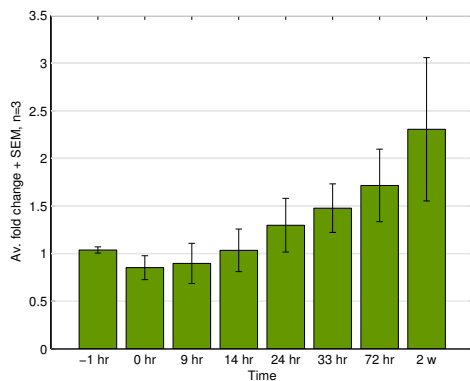
(a) Gene expression of p63.
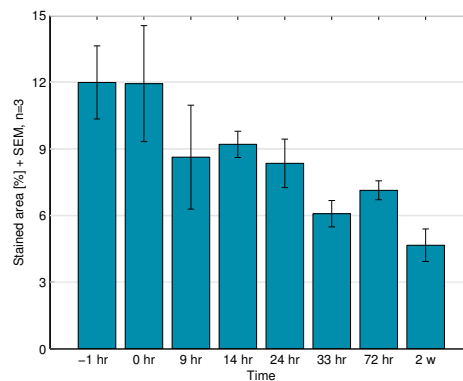
(b) Protein expression of p63.

Figure 28: Analysis of gene and protein expression of basal cell protein p63. Gene expression is visualized through average fold change while protein expression is visualized by image analysis of percent stained area. The graphs are represented by the three different donors.

Visual investigation of samples stained for p63 showed positive stained cells adjacent to the wound edge. Further investigation showed basal cells covering large parts of the healed wound area, see figure 29a and figure 29b.
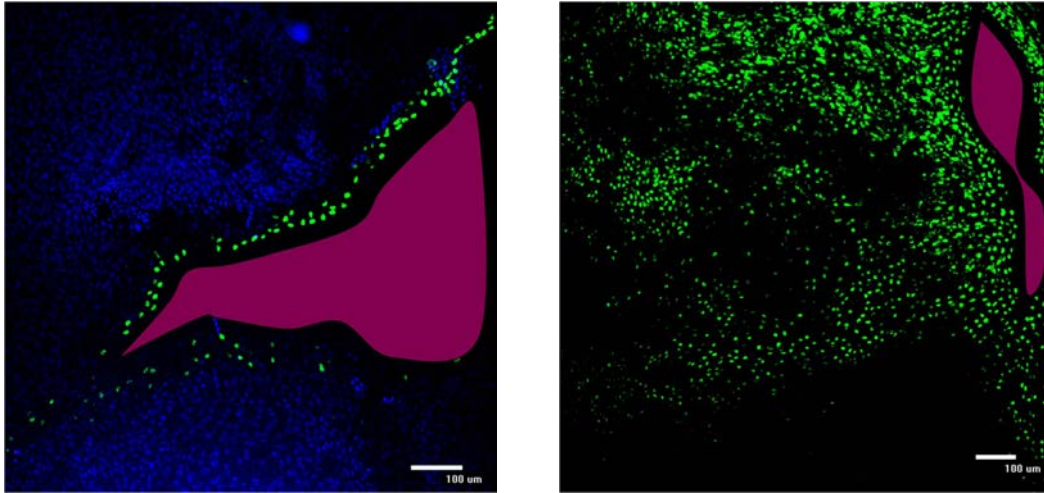
(a) Basal cells adjacent to wound edge.

(b) Basal cells covering healed area.

Figure 29: Immunofluorescent staining of basal cells showed in green. Open wound areas are marked by a purple mask. In figure (a) DAPI was used to stain all cell nucleus in the cell culture, shown in blue.

The expression of mucin MUC5AC was investigated both through gene expression and protein expression. Gene expression showed an increase in expression during 9 hours and 14 hours post wounding followed by stabilized expression comparable to normal levels, see figure 30a. Protein expression was investigated through image analysis of immunofluorescent stained samples showing comparable result to the gene expression, with an increase of protein expression at 9 hours and 14 hours, followed by a decrease and stabilized normal expression levels again, see figure 30b.
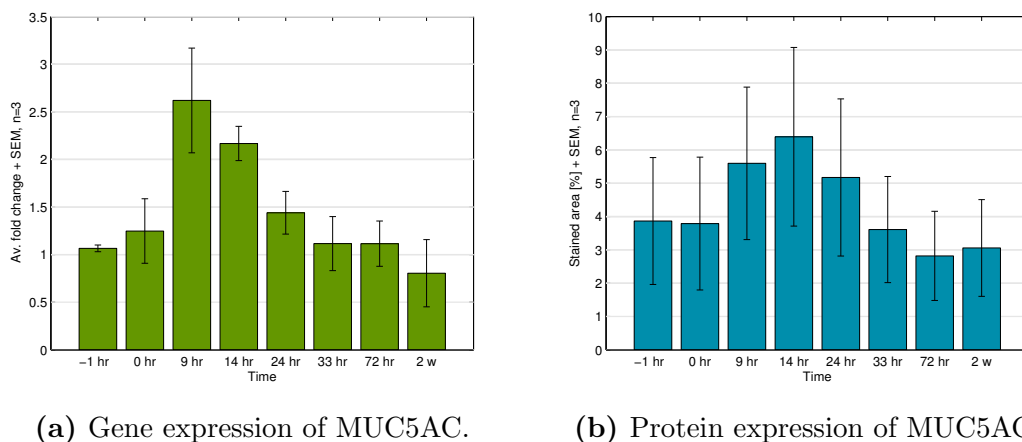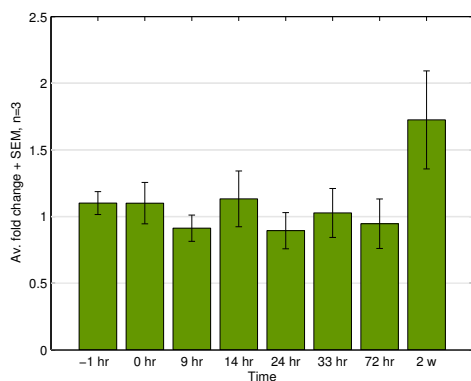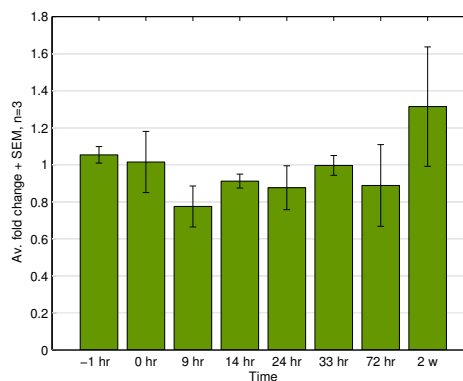
(a) Gene expression of MUC5AC.

(b) Protein expression of MUC5AC.

Figure 30: Analysis of gene and protein expression of goblet cell MUC5AC mucin. Gene expression is visualized through average fold change while protein expression is visualized by image analysis of percent stained area. The graphs are represented by the three different donors.

Ciliated cells were investigated by analysis of gene expression of FOXJ1, SP17 and TUBB4. FOXJ1 and SP17 showed stable expressions over time with an increase in expression at two weeks. TUBB4 showed an increase in expression at 14 hours followed by a stable and slightly decreased gene expression, see figures 31a, 31b and 31c. Protein expression of both FOXJ1 and TUBB4 showed small differences over time with an up regulation at 2 weeks, see figure 31d.
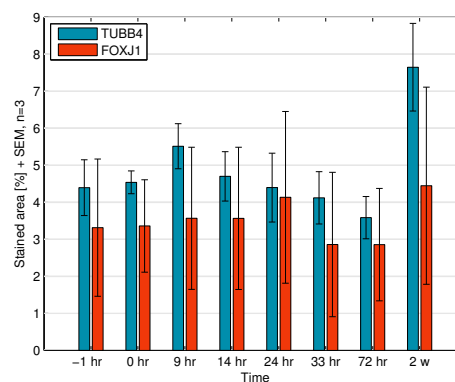
(a) Gene expression of FOXJ1.

(b) Gene expression of SP17.
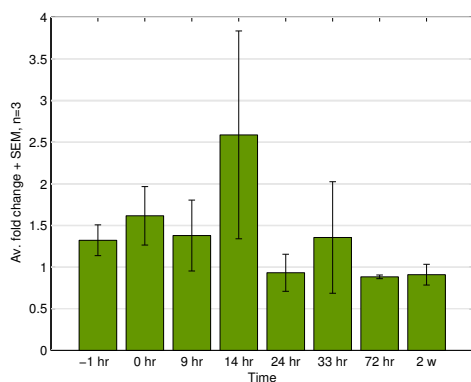
(c) Gene expression of TUBB4.

(d) Protein expression FOXJ1/TUBB4.

Figure 31: Analysis of gene and protein expression of ciliated cells. Gene expression is visualized through average fold change while protein expression is visualized by image analysis of percent stained area. The graphs are represented by the three different donors.

6.3 Smoke assay

NHBE cell cultures exposed to 1:50 volume/volume smoke/air dilution were investigated according to readouts previously described. Following results were collected from the smoke assay.

6.3.1 Physiological barriers

Smoke exposed NHBE cell cultures showed lower TEER values compared to non-treated control cultures. At starting point, all samples showed an equal mean TEER value, see figure 32. After smoke exposure an instant and dramatic drop in TEER was seen.
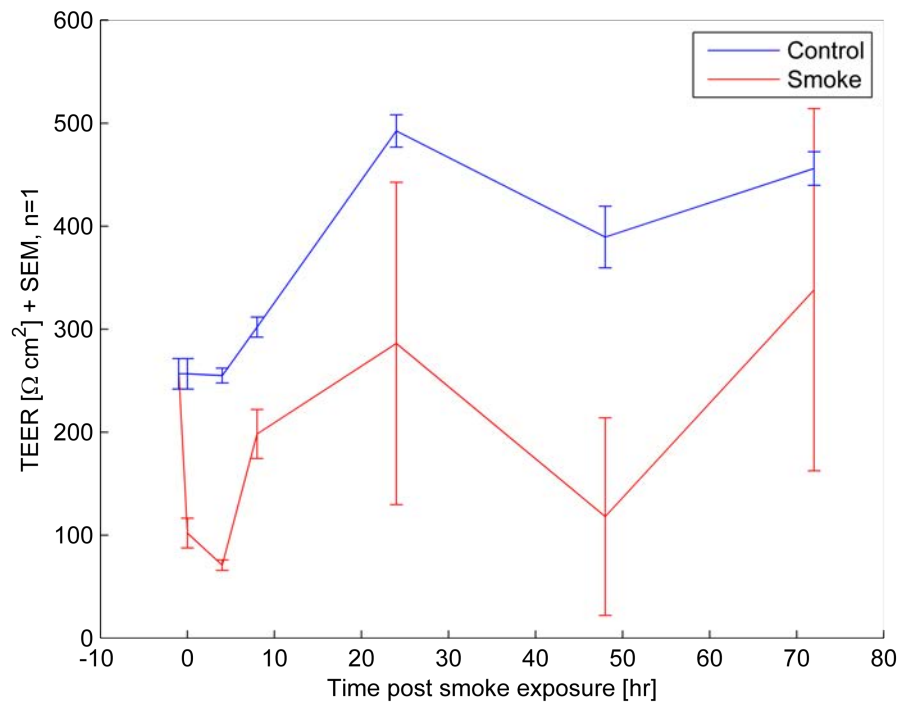

Figure 32: TEER measurement, comparing smoke exposed NHBE cell cultures to non-treated cell cultures.

In connection to obtained TEER results, gene expression of tight junction protein ZO-1 and gene expression of cell-cell adhesion protein CDH1 (E-Cadherin) were investigated, see figures 33a and 33b. Gene expression of ZO-1 was not seen influenced by the smoke, investigating both smoked samples and smoke wounded samples. CDH1 was seen negatively influenced by the smoke, as a down regulation was seen in both smoked samples and smoke wounded samples.
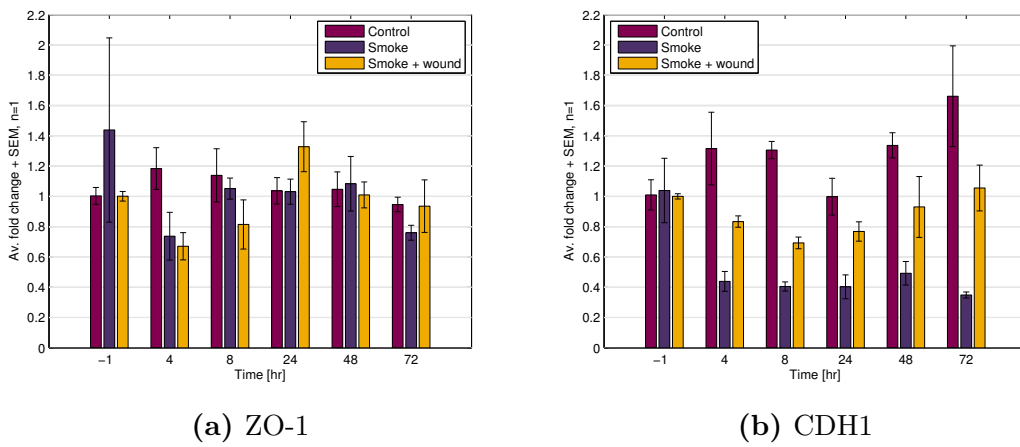
(a) ZO-1

(b) CDH1

Figure 33: Gene expression of tight junction protein ZO-1 and cell-cell adhesion protein CDH1 comparing smoked samples and smoke wounded samples to control samples.

6.3.2   Cell migration

Results obtained using the Cell-IQ system showed a delayed migration by smoke wounded cell cultures with several hours compared to wounded controls, see figure 34. Mean values for wound closure, donated with stars in figure 34 showed delayed wound closure with almost 41 hours.
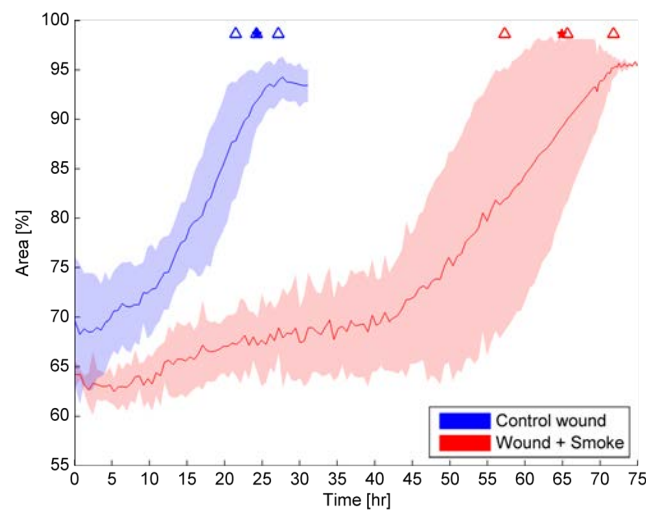

Figure 34: Cell migration of smoked samples versus controls. Stars represents the mean closure time and triangles individual closing of each sample.

Gene expression of MMP-9, connected to migration, showed a down regulation in smoked samples whereas the smoke wounded samples showed a slight up regulation at 48 and 72 hours which corresponded to the migration seen by the Cell-IQ analysis, compare figure 34 with figure 35.
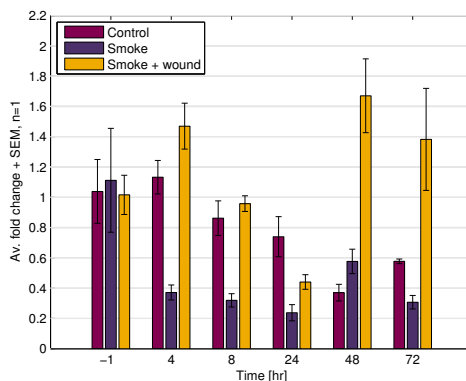

Figure 35: Gene expression of MMP-9, a matrix metalloproteinase linked to cellular migration in bronchial epithelial cells, comparing smoked samples and smoke wounded samples to control samples.

6.3.3 Cell proliferation

Gene expression of KI-67 showed an instant down regulation of proliferation in smoked samples during the whole experimental time, while the smoke wounded samples showed a down regulation to 24 hours followed by an upregulation, see figure 36.
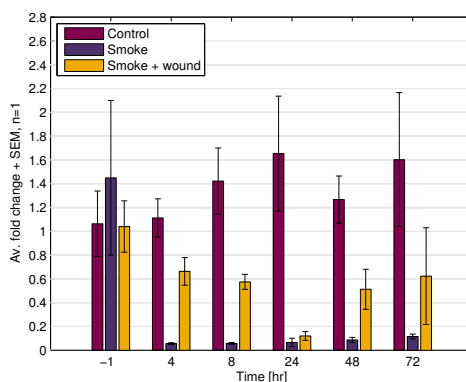

Figure 36: Gene expression of proliferation protein KI-67, comparing smoked samples and smoke wounded samples to control samples.

6.3.4   Cellular stress response

Gene expression of three different stress relate genes; DDIT3, HSPA6 and TXNRD1 showed the common feature of smoke wounded samples expressing a higher stress response compared to smoked samples. Smoked samples showed stress response with upregulation of TXNRD1 and HSPA6, while DDIT3 showed a slight down regulation over time.

(a) DDIT3

(b) HSPA6

(c) TXNRD1
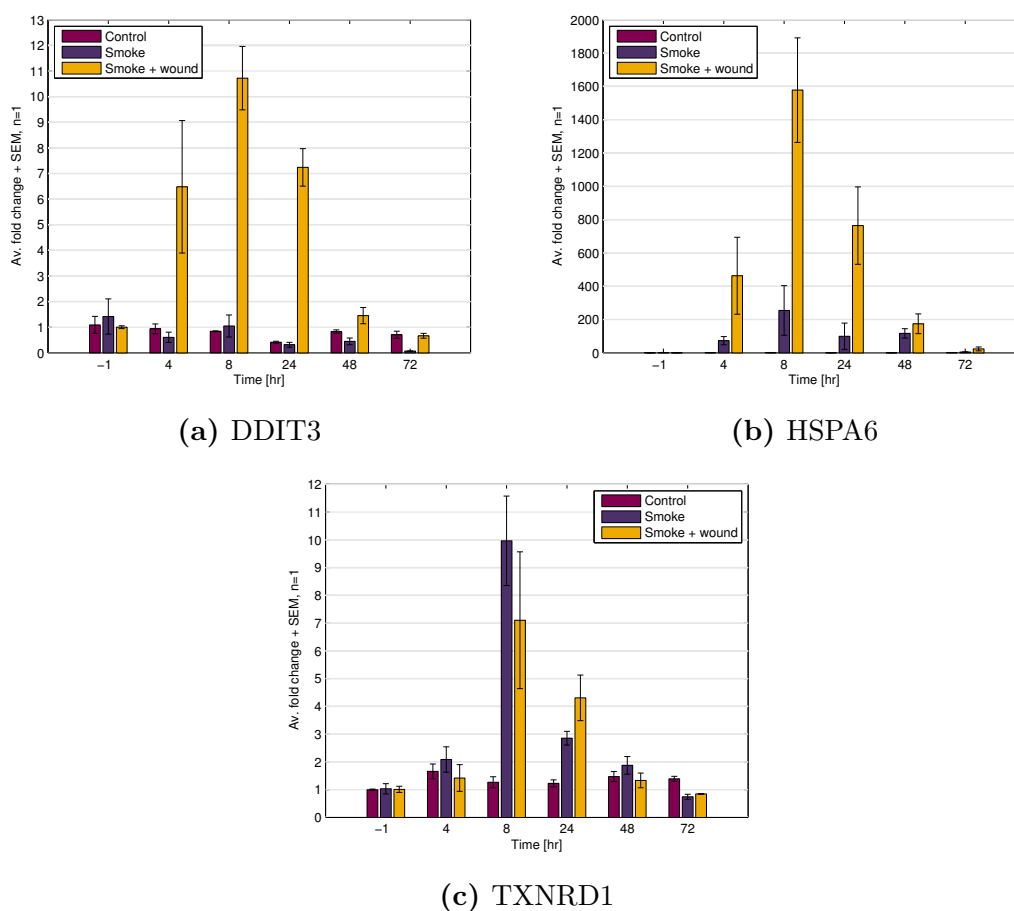
Figure 37: Gene expression of stress related proteins, comparing smoked samples and smoke wounded samples to control samples.

Cell apoptosis investigated through gene expression of caspase-3 showed a drastic down regulation in smoked samples and a slight down regulation in smoke wounded samples, see figure 38a. The quick and dramatic decrease in gene expression, was not seen in smoked wounded cultures, which showed a delayed response seen at 48 and 72 hours. Investigating gene expression of IL-8, a down regulation in smoked

samples and a tendency of up regulation in smoke wounded samples was seen, see figure 38b.

(a) Caspase-3

(b) IL-8
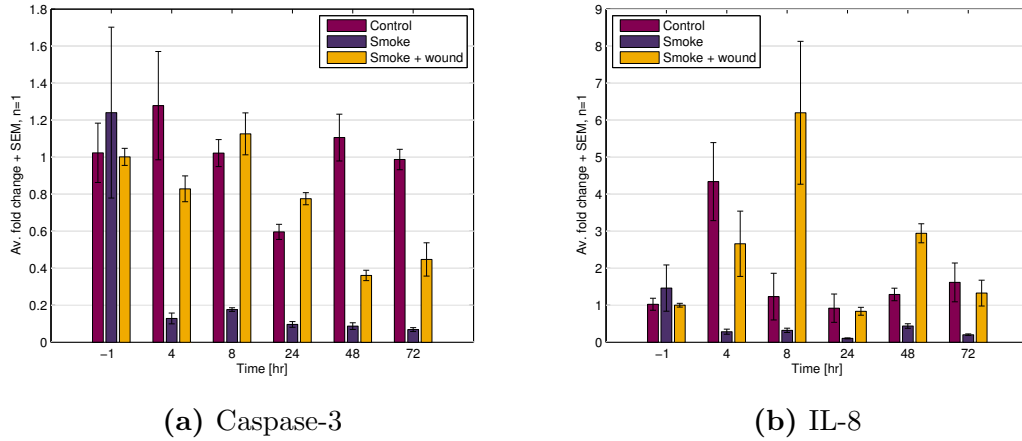
Figure 38: Gene expression of apoptosis protein Caspase-3 and chemokine IL-8, comparing smoked samples and smoke wounded samples to control samples.

6.3.5 Cell populations

Gene expression of the three different cell types; goblet cells (MUC5AC), ciliated cells (FOXJ1) and basal cells (p63) are seen in figure 39a-39c. FOXJ1 was seen to have a drastic down regulation in smoked samples and a slight down regulation in smoke wounded samples. Expression of p63 showed not any clear tendency at the investigated time periods and seemed stable over time. The MUC5AC showed a down regulation in all smoked samples as well as in the control sample.

(a) FOXJ1

(b) p63
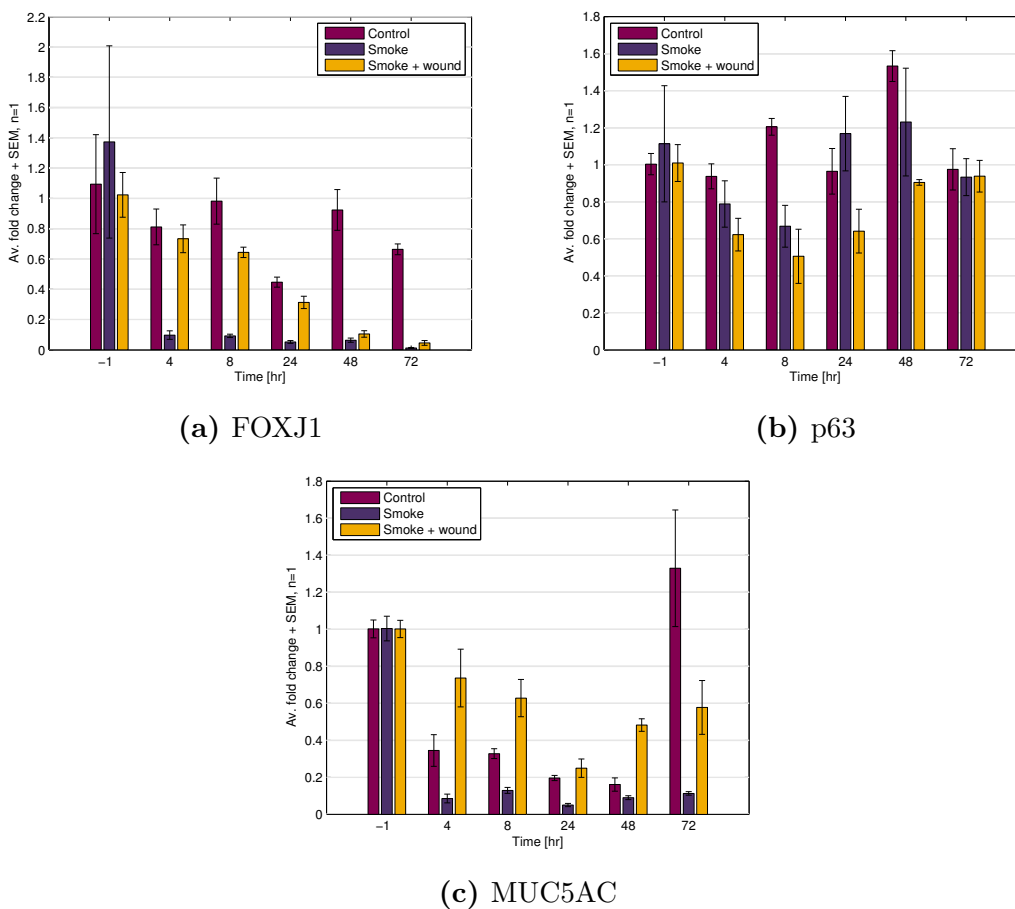
(c) MUC5AC

Figure 39: Gene expression investigating the behaviour of the three major cell types; ciliated cells (FOXJ1), basal cells (p63) and goblet cells (MUC5AC), comparing smoked samples and smoke wounded samples to control samples.

6.4 Compound treatment

The effect of the three different concentrations, 0.1 µM, 4 µM and 10 µM of compound A together with DMSO control to migration can be seen in figure 40. No large differences between the three concentrations as well as to DMSO treated samples was seen. DMSO is represented with floating error bars with a mean curve based on a triplicate.
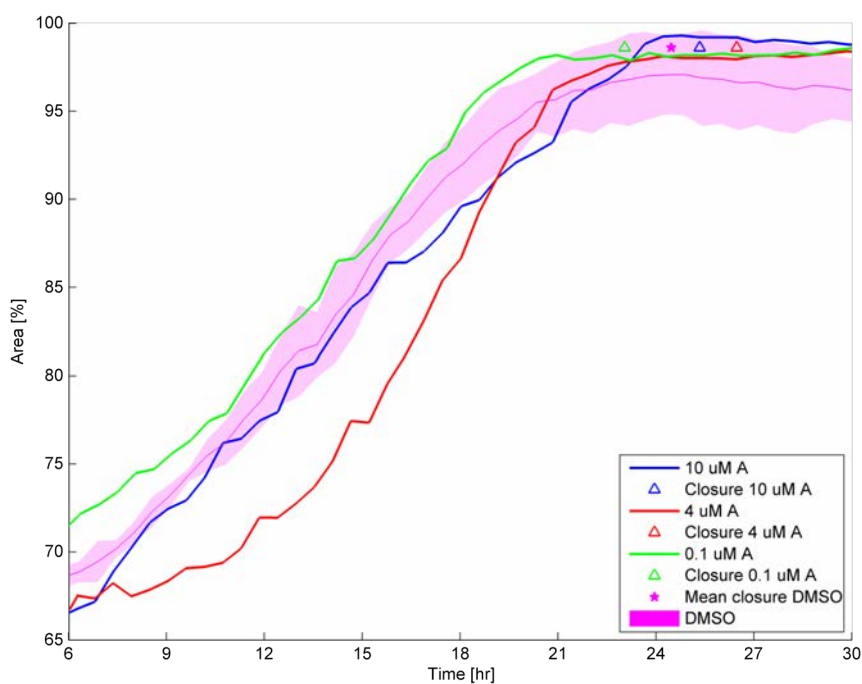
Figure 40: Cell migration of cell cultures treated with compound A, stars representing mean closure time and triangles each individual closing.

Differences between wounded cultures treated with DMSO and non treated wounded cultures could not be determined, see figure 41.
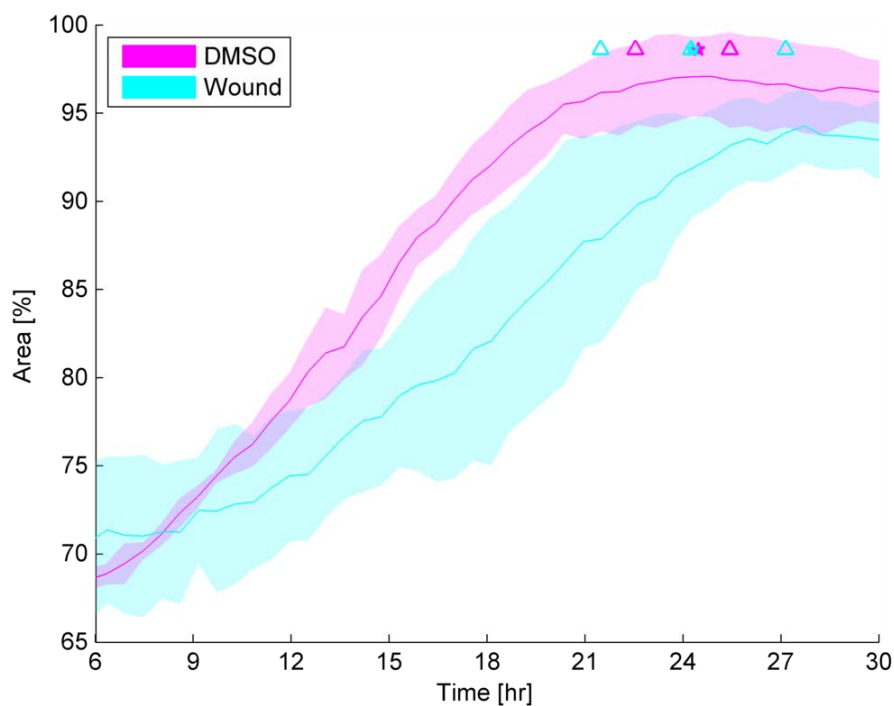
Figure 41: Cell migration of non treated cultures versus DMSO treated.

Migration speed for compound B and positive control compound C did, similar to compound A, not show any major difference from DMSO control and no clear difference between the three individual dilutions. No major difference between the three compounds could be determined. Figures representing the migration for compound B and positive control compound C can be seen in Appendix F, figure F1 and figure F2.

7 Discussion

Following section will cover the discussion and interpretation of the results obtained from the method evaluation, scratch assay, smoke assay and compound treatment.

7.1 Method evaluation

The discussion of the method evaluation will be divided into smaller parts to easily interpret the results from the different methods.

7.1.1 Scratch wounds

Initial objective of this project was to investigate possibilities to perform a clean and reproducible wound to the NHBE cell cultures cultivated on Transwell inserts in ALI. Implant of small obstacles such as plastic blocks, or small strips of materials to be ripped away and thereby tear away the cells above it, were rejected. The cell culturing can be seen as a slow process and needs approximately 28 days of cultivation until fully differentiated and ready for experiments and the implant of obstacles or strips would exclude the cultures to be used for any other experiments except wound and migration assays. Using a strip would also add more complexity to the model as the cells need to have contact with the basolateral medium in order to live, causing the strip to be made of a permeable material. From these arguments, the wound had to be performed in conjunction to the experiment to allow larger flexible decisions. Ideas of performing wounds through freezing or burning off the cells were neglected with aspects of risk of destroying the membrane as well as not simulating *in vivo* like damage based on the disease area. Performance of scratch wounds, a common used technique [52, 57–61], were investigated by different tools. At an early stage it was concluded that Pasteur pipettes were able to produce a continuously scratch wound with distinct wound edges in combination with the removal of eliminated cells by vacuum suction. The utilization of the scratch technique eliminated all cells in the wound area, a stage different from *in vivo* report of wounds found in asthmatics where the superficial cell layer has seen disrupt, suggesting presence of basal cells in the wound area [38]. An ideal scratch technique would be able to use a reproducible technique, leaving clusters of basal cells in the wound area, to even further mimic the *in vivo* condition seen. Although the removal of all cells is a drawback by the technique used, the scratching technique would in contrast to the usage of obstacles have the advantage of damaging the cells adjacent to the wound edge. Mechanical stimulation have been shown to propagate signals, such as Ca^{2+} waves [32], from stimulated cells to adjacent cells,

where the propagation of signalling could influence a large amount of cells in the culture. This signalling has not been further investigated in this project, but a theory is that the scratch simulates a greater stress compared to the removal of an obstacle. The glass pipette was however seen to damaged the membrane (figure 9) as a result of the scratching. The damage was after visual investigation not considered large enough to exclude the proposed scratch method from the project.

7.1.2 Antibody evaluation

In order to analyse changes in protein expression over time immunocytochemistry techniques were used. Antibodies were evaluated for their specificity and it was early discovered how a majority of the antibodies did not show any signal or abnormal signal by non specific binding. Antibodies specific to cell types of ciliated (FOXJ1, TUBB4 and SP17), goblet (MUC5AC) and basal cells (p63) were identified as well as marker for tight junction protein ZO-1 and proliferation marker KI-67. To evaluate any presence of Clara cells in the cell culture, an antibody for Clara cell secretory protein (CCSP) was used. As no signal was seen in the NHBE cell cultures, validation of the CCSP antibody was performed, resulting in a positive signal, in human alveolar tissue (figure 10f). The CCSP antibody was evaluated on alveolar tissue to exclude any presence of Clara cells in the cultures as bronchial epithelium is composed of goblet, ciliated and basal cells [7, 8].

By the evaluation it was decided that different combination of markers (table 6) should be used to reduce the amount of culture samples needed to investigate the protein expression. Proliferation marker KI-67 was used in combination with basal cell marker p63, to investigate any proliferation within the population of basal cells. FOXJ1 was used in combination with TUBB4 to investigate if all ciliated cells expressed cilia, and MUC5AC in combination with TUBB4 to investigate if any visible connection between goblet cells and ciliated cells could be made.

The combination of FOXJ1 and TUBB4 for visualization of ciliated cells through immunofluorescent staining showed FOXJ1 positive cells expressed cilia (figure 12a). Immunofluorescent staining with SP17 (figure E1 in Appendix E) did, as seen by immunoperoxidase staining, show positive staining of cilia and the cytoplasm of ciliated cells. The non-specificity binding excluded the SP17 antibody for further use in the project. However, as SP17 was found specific to ciliated cells, the usage of SP17 could be adapted and evaluated in gene expression assays. Immunofluorescent staining of basal cells showed a difference in expression when comparing 7 day old culture compared to 39 day old culture (figure 13). The decreased expression of basal cells at day 39 compared to day 7 could be a result of basal cells ability to differentiate into other cell types. Investigating im-

munofluorescent images of tight junction protein ZO-1 in young cultures, at day 7, showed small areas of tight junction formation compared to older cultures. At day 30, staining showed a continuous expression seen in the whole culture (figure 14). Using the proposed ICC technique, ZO-1 could potentially be used to follow and determine the maturation of tight junctions over time.

The double-staining of proliferation marker KI67 and basal cell marker p63 showed proliferative cells positive stained for p63 (figure 15b), strengthen the theory of basal cells are responsible being the proliferation in bronchial epithelium [24, 25].

By comparing the location of goblet cells and ciliated cells, MUC5AC and TUBB4 immunofluorescent staining, in several different donors (data not shown in the report) no distinct correlation between the location of the two cell types could be determined. Visual inspection indicated goblet cells and ciliated cells to be located together in patches, often found closer to the wall of the well, whereas other donors had an even distribution of the two cell types in the whole culture.

7.1.3   Trans epithelial electrical resistance

Evaluation of the two different electrode devices used to conduct TEER measurement indicated no distinct difference (figure 16). The Endohm 6mm Culture Cup was easy manageable and was independent of the operator conducting the measurements, resulting in the choice to be used for oncoming measurements. The STX2 Chopstick Electrodes were on the contrary not easy manageable, the cell culture was easily scratched with the apical electrode and as the electrodes were flexible, maintaining constant distance between the two during measurements was challenging.

7.1.4   Cell-IQ

The Cell-IQ was early concluded to be a functional tool to analyse cell migration in epithelial ALI cultures. As the cell sheet was transparent and the Transwell membrane was seen through the cells, an issue was raised during the analysis in order to distinguish the difference between the cell sheet and the membrane. By building larger sample libraries the sensitivity increased. Analysis of one wound closure, composed of 423 images covering 48 hours image sampling, required approximately 24 hours of analysis. The analysis was shown to be time consuming and could not be used as a high through put system and required large amount of time in order to receive good results.

During the evaluation, non-wounded cell cultures were investigated as well to investigate the Cell-IQ's potential to monitor regular cell cultures. The results were surprisingly, revealing a constant cellular migration within the cell culture. This migration has, to the writer, not been previous reported. The underlying factor for the migration was not further investigated in this project. Further experiments could however investigate the impact of different coatings of the membrane, such as other types of collagens, to the migration.

Analysis performed by Alan Sabirsh[6] did show an alternative image analysis to be used for non-wounded ALI cultures (figure 18). Using this analysis methods would promote the possibility to track cell migrations in various assays and could, in future experiments, potentially be used to track responses of stimuli of different irritants, such as smoke or other inhaled compounds.

7.1.5   Smoke exposure

The evaluation of smoke exposure to the ALI cultures, 1:50 volume/volume smoke/air dilution was chosen for oncoming experiments, as it did not show any severe cell death compared to the 1:5 and 1:10 dilutions (figure 19). The setup of peristaltic pumps for distribution of fresh medium and removal of old medium worked properly (figure 6) and hopefully the same setup could be used, in future experiments, to perform chronic smoke exposure experiments. To mimic normal culturing conditions during chronic smoking the addition of switching the smoke inlet to a CO_2/air mixture between smoke exposure would be necessary.

7.2   Scratch assay

The wound healing progression from the scratch assay was observed according to the stages presented in figure 3: dedifferentiation, migration, proliferation and redifferentiation. A healthy epithelium was wounded by mechanical scratching using the scratch method used in the method evaluation. The dedifferentiation was not investigated in this project. Stainings of fixated cell cultures showed positive staining of basal cells adjacent to the wound edge (figure 29a). As cells close to the wound edge dedifferentiate before migrating, the positive staining of basal cells could be the result of dedifferentiation of goblet and ciliated cells.

Migration, the second step in epithelial wound healing, was monitored through the Cell-IQ's image analysis revealing a variation between the three donors as well

---

[6]Alan Sabirsh, Image expert, CVMD, AstraZeneca R&D Mölndal

as variation within the samples of each donor (figure 23). Visual video analysis revealed a migration performed by the whole cell sheet rather than a few cells, a result not comparable to previous reported results of scratch assay of monolayer cultures where migration have been documented not to be seen at a distance further than 1.6 mm from the wound edge [62].

By using the scratch assay, a limitation is raised in controlling the surface membrane composition. As the cells are removed through mechanical scratching, nothing is known about the surface membrane. Before culturing the cells, the membrane is incubated with collagen I and III in order to mimic the *in vivo* basement membrane. After scratching the collage and other ECM proteins, expressed by the cell culture during cultivation, could have been removed to an unknown extent. The variations in migration could potentially be linked to the cells ability to migrate onto the nude membrane and the rate of expressing new ECM proteins. Investigations of the membrane composition could be done in future experiments to conclude potential effect to the migration speed. The cells left on the membrane, not removed by the scratching, should be connected to ECM proteins located on the membrane surface by different adhesions. In order for a cell to start migrate the adhesion has to be disrupt. MMP-9, a matrix metalloproteinase, has been suggested to be involved in the migration of airway epithelial cells [48]. Previous studies, observed by monolayer cell cultures of HBEC and HNEC, has shown increased levels of MMP-9 during wound healing. The upregulation of MMP-9 has shown to be extensive in migrating cells adjacent to a wound edge and to be expressed throughout the wound healing. These results suggested the ability of MMP-9 to cleave contacts between lamellipodia and collagen IV and thereby promote migration through new contacts in the front of the direction of cell migration. Blockage of MMP-9 has been shown to reduce the migration speed drastically [52, 53].

The gene expression of MMP-9, observed within the three donors, showed an upregulation between 9 hours and 72 hours post scratching (figure 24). By comparing the expression of MMP-9 with the image analysis data, it was concluded that MMP-9 was upregulated during the visual migration of the three donors. As blockage of MMP-9 has shown reduction in migration speed in submerged HBEC cultures, future experiments could investigate the effect of both blockage and induction of MMP-9 in ALI cultures.

As the cells starts to migrate, the pseudostratified cell composition is caused to adapt a more squamousness formation. This formation change was investigated by the expression of cornifin A and involucrine (figure 25). Involucrin and cornifin A was used as markers for squamous metaplasia, where involucrin has been found expressed in stratified squamous epithelium [84, 85] and cornifin A in the suprabasal

layer of epidermis [86]. The expression of involucrin and cornifin A showed an up-regulation the first 14 hours post scratch wound, followed by a decrease of cornifin A whereas involucrin showed large variation in the data. The decrease seen by corifin A can be connected to the increase in proliferation (figure 26a). As an increase of cells in the culture would result in less space for squamous cells, the proliferation could promote a change in cell phenotype to a pseudostratification confirmation.

Proliferation, the wound healing step following the migration, was investigated by gene expression of KI-67 (figure 26a). The increased expression of proliferation seen by KI-67 correlates with the Cell-IQ data and occurs in close time to complete migration. Unfortunately, image analysis of ICC stained KI-67 samples (figure 26b) showed fluctuations in the data, but could to some extent confirm the gene expression data. Gene expression of KI-67 was also compared to gene expression of PCNA (figure 27), which did not show any change in expression.

Comparing the increase in gene expression of KI-67 (figure 26a) over time to gene expression of basal cells (figure 28a), a similar behaviour was seen. The increase in proliferation was consistent with an increase in gene expression of basal cells. The protein expression of basal cells, investigated by image analysis of ICC stained samples, showed a decrease in basal cells over time. It was also observed, examining the fixated samples, that large amounts of basal cells were located covering the healed wound area (figure 29b). Visual comparison to ICC samples of goblet cells and ciliated cells, data not shown, basal cells were seen predominant located in newly covered wound areas. This observation further strengthen the theory of basal cells acting as the progenitor cell type [87]. A potential difference between the ICC data and gene expression data could be explained by the difference of the presented data. One analysis representing the gene expression, the other protein expression. As not all mRNA need to be translated to proteins, it might be hard to truly link the two analysis data. The extent of mRNA actually translated into protein is unknown as well as the time from mRNA to fully functional protein. Another action to consider is the manual performed image analysis, where the misfit result could be explained by not representing the whole cell culture.

The last wound healing step, the redifferentiation, was investigated through a combination of readouts. Instigations of the two major cell types, goblet and ciliated cells, revealed an upregulation of MUC5AC mucins during 9 hours and 14 hours through increased levels of both gene and protein expression (figures 30a and 30b). This upregulation could be a response to the scratch wound, where an increased amount of mucins and thicker mucus would trap foreign particles or intruders and by the entrapment transport it away from the epithelium minimizing the risk of leaving the intruder entering the wound. The ciliated cells did not show any re-

action to the scratch wound, showing similar profile patterns examining the gene expression of FOXJ1 (figure 31a) and SP17 (figure 31b) as well as protein expression of FOXJ1 and TUBB4 (figure 31d). An increase of the cilia markers was seen at 2 weeks post scratch wound, both through gene and protein expression of ciliated cells. The increase could be explained by maturation of the cell cultures where long time cultivation has, through visual inspection, shown an increase of cilia over time. The gene expression of TUBB4 (figure 31c) showed a non-similar behaviour, where an increased expression was seen 14 hours post scratching. Tubulin is known to be expressed as a cytoskeletal protein [19], suggesting the result to represent the migration rather than the cilia formation as image analysis of TUBB4 stained samples revealed staining of the cytoskeleton (figure E3 in Appendix E).

TEER was regulary measured during the cultivation and wound healing of the cell cultures. The resistance could be seen located between 400-1000 $\Omega \cdot cm^2$ during differentiation (figure 20). Introducing a scratch wound caused a dramatically drop in resistance to approximately 40 $\Omega \cdot cm^2$. Monitoring the wound healing, it was seen that although the wounds were visually closed the resistance still increased, suggesting the physiological barriers not to be fully established at wound closure. The gene expression of tight junction protein ZO-1 showed no changes over time (figure 22a). ICC stained samples of ZO-1 showed strong signal close to the wound edge with a pattern comparable to a non-wounded culture, compare figures 14a and 22b. Even though the TEER measurements revealed a clear negative impact on the physiological barriers and thereby also the tight junctions, the tight junction protein ZO-1 seems to be mildly affected. Further experiments could be done to investigate if other tight junction protein are affected to a greater extent by the scratch wound. As no correlation could be made between the TEER and ZO-1 data in this project and the ZO-1 activity is presented to be associated with high resistance [30], further experiments could also include if any correlation can be made between cell density and TEER. The TEER measured during wound healing showed an increasing resistance after visual wound closure which could be a result of the cell proliferation. Examining any correlations between cell density and TEER could reveal if the increase is caused by the cell proliferation or by formations of tight junctions.

Summarizing the results from the scratch assay, it could be seen that the cell cultures recovered and healed during the 2 week time period investigated. Basal cells were seen lining the border between cell culture and wound, comparable to previous reported findings [53]. The migration was monitored through live imaging, revealing a migration caused by the whole cell sheet rather than by a few migrating cells. The removal of cells for creation of wounds were seen causing a squamous cell confirmation which during healing decreased, after the migration and closure of the

wound, with increased levels of proliferation. The proliferation could be connected to increased levels of basal cells. Large amount of basal cells were found in the wound area, a result supported by theories of basal cells acting as the multipotent progenitor cell type [87]. Ciliated cells seemed not to be affected over time by the scratch wound, where as goblet cell showed an upregulation of mucins during the wound healing.

7.3   Smoke assay

Compared to the scratch assay, the smoke assay was evaluated with some differences. The migration, proliferation and dedifferentiation (figure 3) were investigated in similar manner as to the scratch assay. In the smoke assay additional gene markers were investigated while the ICC was rejected as a result of the large time frame required for analysis.

To mimic the behaviour of smoking, ISO standards for cigarette smoking was used in combination with the Borgwald RM20S smoking robot, a machine documented to generate accurate and reproducible smoke doses [72]. Cigarette smoke was generated from Kentucky reference cigarettes, a common used cigarette type in *in vitro* experiments [88]. Although the reference cigarette is not used by smokers *in vivo* it offers the possibility to reproduce and compare experiments, performed both *in vitro* and *in vivo*, by generating similar smoke from each cigarette used. Using commercial available cigarette, and thereby use the smokers choice of cigarette, could lead to an ethical dilemma for pharmaceutical companies. If purchasing cigarettes directly from the tobacco industry, it could be seen as a standpoint and sponsorship of a certain company. The reference cigarettes offers a research cigarette and are offered and sold solely for research purposes and are not for human consumption.

The smoke assay started with exposing scratch wounded cell cultures to a dilution of 1:50 smoke/air. The migration was investigated through the Cell-IQ system, which revealed a major effect of the cigarette smoke to the cellular migration. The migration of smoke wounded cell cultures showed a delayed wound healing with almost 41 hours (figure 34). Although cigarette smoke delayed the migration, the curve profile seen was similar to the control where the delay in migration could be seen as a lag phase. The Cell-IQ data was compared to the gene expression of MMP-9, showing an upregulation at 48 hours and 72 hours (figure 35). The upregulation was connected and identified with the increased migration from the Cell-IQ data. MMP-9 has previous been suggested linked to cellular migration in HBEC cultures [48]. The result of smoke affecting migration was confirmed

by non-wounded cell cultures, where the expression of MMP-9 was sustained low throughout the experiment compared to control samples (figure 35).

The proliferation, the wound healing step following the migration, was investigated through gene expression of KI-67. The smoke showed a large down regulation in proliferation in smoked cell cultures, while smoke wounded samples showed less down regulation (figure 36). The higher proliferation expression by smoke wounded samples could be explained due to proliferation occurring in conjunction to the wound healing. The gene expression of basal cells, acting as the multipotent progenitor cell type [87], did show a slight down regulation followed by an upregulation analysing both smoke wounded and smoked cell cultures (figure 39b).

The redifferentiation was assessed by investigation of the gene expression of goblet and ciliated cells. Ciliated cells were seen down regulated in both smoke wounded and smoked cell cultures (figure 39a) which coincides with *in vivo* observations of cigarette smoke causing destruction of cilia [8]. The expression of goblet cell mucins showed a down regulation over time in both smoke wounded and smoked samples (figure 39c). As the control sample suffered of a large down regulation and the result is in contradiction to previous reported data, presenting cigarette smoke as a trigger for mucus production and release [8, 39, 40], the result from the MUC5AC experiment was seen as invalid.

The cellular stress response from cigarette smoke was assessed through investigation of gene expression of heat shock protein 70 kDa (HSP70B or HSPA6), DNA-damage-inducible transcript 3 (DDIT3) and thioredoxin reductase 1 (TXNRD1). HSP70B has shown to be important for cell viability during accumulations of damaged proteins [89]. DDIT3 has shown to inhibit migration and proliferation depending on location in the cell cytoplasm or nuclei [90], while the expression of TXNRD1 has been linked to oxidative stress defence mechanisms [91]. All three genes were elevated in smoke wounded samples as well as in smoked samples with exception of DDIT3 (figure 37). Expression of DDIT3 was seen stable for smoked cultures, a result contradictory to previous reported data suggesting cigarette smoke causing elevated levels of stress related signals [43]. Interestingly a larger stress response could be seen to the smoke wounded cultures compared to the smoked cultures. Expression levels of the cytokine interleukin-8 (IL-8) has been reported to increase, caused by the inflammatory response, by cigarette smoke [44, 45]. The gene expression of IL-8 did unfortunately not support the theory, revealing a down regulation seen by smoked cultures (figure 38b). Smoke wounded samples showed a fluctuating regulation of IL-8, perhaps as a inflammatory response to the mechanical scratching.

Potential cell death was initially planned to be monitored through cell apoptosis

and the expression of caspase-3, a protease connected to activation of cell death. It was however discovered that caspase-3 levels were significant down regulated in smoked cell cultures and slightly down regulated in smoke wounded cultures (figure 38a). Cigarette smoke was later discovered to have been reported not to induce caspase-3 in bronchial epithelial cells [67]. Accordingly, the gene expression of caspase-3 showed a down regulation in both smoked and smoke wounded cell culture (figure 38a).

The TEER was measured continuously to observe any changes to the physiological barriers caused by the smoke exposure. Instantly after smoke exposure the resistance decreased and sustained low over the time period investigated (figure 32). As cigarette smoke has shown to decrease expression of both cell-cell adhesion protein epithelial cadherin (CDH1) [41] and induce disassembly of tight junction protein ZO-1 [42], the gene expression of both ZO-1 and CDH1 was investigated. Expression of ZO-1 revealed a very small down regulation at 4 hours followed by a constant expression (figure 33a). The gene expression of CDH1 (figure 33b), showed a decrease expression in smoked samples, while the expression was seen higher for smoke-wounded samples, suggesting a disintegration of cell-cell contacts.

Summarizing the smoke assay, the cigarette smoke was seen to negatively affect the migration and proliferation. The TEER was instantly negatively affected, not fully recovering during the investigate time frame and a disintegration of cell-cell contact was suggested. Several stress responses were identified in the cell cultures, both for smoked samples as well as for smoke wounded samples.

7.4 Compound treatment

Suggestions were made from toxicologists, at a department working with drug safety issues at AstraZeneca R&D, to evaluate the scratch assay model combined with exposure of three different compounds. A first experiment was conducted by applying compounds apically to the wounded cell cultures and monitoring the migration using the Cell-IQ system. Analysing the migration profiles for compound A (figure 40), B (figure F1 in Appendix E) and positive control C (figure F2 in Appendix E), no significant differences between the compounds or the different concentrations could be made. As DMSO is known to be toxic to cells [92], the effect of the DMSO was compared to negative control (figure 41) revealing no difference in time of wound closure. However, a difference in curve shape was seen, which could be a result of non sufficient image analysis by the Cell-IQ system.

As no impact was seen by the different compounds, further experiments need to be performed. Suggestions from the toxicologist were made as the compound

concentrations were concluded to be too low. Further experiment can be made with concentrations up to 400 µM, compared to the used 10 µM maximum dose, in order to evaluate effects on cellular migration.

8   Conclusions

By this project a successful model for wound healing using primary NHBE cell cultures has been established. The cell cultures were concluded having a high recovery towards mechanical scratching and whole cigarette smoke exposure analysing physiological barriers, re-establishment of cell populations, functional cellular migration and proliferation. Through this project a combination of different readouts were used to accurate follow the healing processes of the cell cultures. Through ICC techniques, several antibodies were evaluated and identified for visualisation of different cell types as well as tight junctions and proliferative cells. Evaluating methods for live imaging of the NHBE cell cultures revealed a significant background migration constantly occurring in fully differentiated cell cultures.

Basal cells, thought as the cell type responsible for proliferation and differentiation within the cultures, were noticed lining the wound edges of scratch wounded cell cultures. Furthermore, basal cells were seen to be the predominant cell type present in healed wound areas up to 72 hours post scratching. Double-staining visualized basal cells as positive stained for proliferation marker KI-67, supporting the theory of basal cells acting as the cell type responsible for proliferation and differentiation within the NHBE cell culture.

Through evaluation and development of a protocol to whole cigarette smoking, a successful set up was established for delivering cigarette smoke to the NHBE cell cultures in ALI, with a continuous medium fed to minimize effects of accumulation of cigarette smoke in the culture medium. The effects of an acute smoke exposure were evaluated whereas the possibilities to perform chronic smoke exposure has to be further evaluated. The cigarette smoke showed a major negative effect to the migration, proliferation and physiological barriers. Through gene expression analysis a distinct stress response could be determined within both smoke exposed cell cultures as well as scratch wounded smoke exposed cultures. Following the cellular migration of scratch wounded cell cultures exposed to cigarette smoke, a distinct lag time was determined compared to scratch wounded cell cultures not exposed to cigarette smoke. This significant lag time could potentially be used to investigate pharmaceutical compounds or cellular pathways response to cellular migration.

The model used in this project should provide useful information for future development of wound healing assays performed through scratch assay, cigarette smoke exposure or a combination of the two. The analysis tools and results presented by this project can serve as a base to future studies of NHBE cell cultures.

9 Future work

Visions of future work for this project could be proceeded through a number of different ideas. Following section will cover some ideas for refinement of the project as well as new paths to discover.

As the evaluation of the model for compound treatment did not show any clear effect, it would be interesting to do further experiments with higher compound concentrations in order to analyse potential effects to the cellular migration.

The upreuglation of MMP-9 seen during cellular migration could be used as reference data to investigate changes in migration through inhibition or stimuli of MMP-9 to scratch wounded cell cultures. By continuing development and refinement of the analysis method suggested by Alan Sabirsh presented in evaluation of the Cell-IQ system, the cellular migration could be analysed without introduction of scratch wounds to the cell cultures.

The wound healing model could be used to evaluate primary cells from asthmatics and COPD donors and thereby compare differences between disease cultures to the normal healthy cultures used in this project. The evaluation could reveal if the material collected from the disease donors is composed of a mixture of healthy and diseased cells as the cryopreservation of the cells could perhaps lead to the death of the disease cells, resulting in a culture with mixture of more healthy cells. To determine the state between disease and healthy cell material a first step could be to cultivate and investigate differences between cell populations, TEER, protein and gene expression. If the results suggest differences between the disease and healthy donors the scratch assay could be used to investigate migration and proliferation in order to study effects of the disease connected to cellular function. However, the possibility of losing the disease phenotype in materials from disease patients should be considered during the cultivation. If there are no major differences between the normal, asthmatic and COPD donors, different treatments of healthy cells could be evaluated in order to simulate of the disease states. Developing methods for chronic smoking could be used to evaluate a disease response over time comparable to COPD. Similar, disease relevant simulation of such as IL-13, an interleukin shown to be linked to allergen-induced and non allergen-induced asthma [93], could be used to simulate and trigger the conditions of asthmatics.

To rationalize and automate the introduction of wounds to cell cultures, another base for performing wounds could be investigated. By modifying a dispenser device, such as a Multidrop, a defined small volume of a chemical, such as NaOH, followed with washing steps could be precision dispensed to each cell culture. NaOH has been documented to successfully produce circular chemical wounds to NHBE

cultures [53, 62]. By using an automated device, the wound could be made independent of performer and hopefully be made with high reproduction during a short time interval. Although the NaOH exposure does not represent wounds seen in an *in vivo* disease state, it could be considered as an option when extensive wounds should be produced under a small time frame.

To develop further complexity to the existing NHBE ALI culture, development of different co-cultures could be studied to even further mimic the *in vivo* situation. Fibroblasts and immune cells could be cultivated together with NHBE cells where the scratch assay and smoke exposure could be used to investigate the effect of co-cultures compared to NHBE cultures.

10   Acknowledgements

References

[1] World health organization: Chronic obstructive pulmonary disease (copd), 2012. URL `http://www.who.int/mediacentre/factsheets/fs315/en/index.html`.

[2] World health organization: Chronic obstructive pulmonary disease (copd), 2012. URL `http://www.who.int/respiratory/copd/en/index.html`.

[3] Barnes P., Drazen J., Stephen I. Rennard M. and Thomson N. *Asthma and COPD: Basic Mechanisms and Clinical Management.* Academic Press, 2009.

[4] Huang S., Wiszniewski L. and Constant S. The use of in vitro 3d cell models in drug development for respiratory diseases. *Tech December*, 2011.

[5] Dvorak A., Tilley A.E., Shaykhiev R., Wang R. and Crystal R.G. Do airway epithelium air–liquid cultures represent the in vivo airway epithelium transcriptome? *American Journal of Respiratory Cell and Molecular Biology*, 2011. 44(4):465–473.

[6] Astrazeneca annual report 2012, 2012. URL `http://www.astrazeneca-annualreports.com/2012/documents/eng_download_centre/annual_report.pdf`.

[7] BéruBé K., Prytherch Z., Job C. and Hughes T. Human primary bronchial lung cell constructs: the new respiratory models. *Toxicology*, 2010. 278(3):311–318.

[8] Tortora G.J. and Derrickson B. *Essentials of anatomy and physiology: international student version.* Wiley, 2010.

[9] Gersh I. Epithelium, 2012. URL `http://www.accessscience.com/content/epithelium/238500`.

[10] Kim K., McCracken K., Lee B., Shin C., Jo M., Lee C. *et al.* Airway goblet cell mucin: its structure and regulation of secretion. *European Respiratory Journal*, 1997. 10(11):2644–2649.

[11] Fahy J.V. and Dickey B.F. Airway mucus function and dysfunction. *New England Journal of Medicine*, 2010. 363(23):2233–2247.

[12] Rogers D.F. The airway goblet cell. *The international journal of biochemistry & cell biology*, 2003. 35(1):1–6.

[13] Alberts B. *Molecular biology of the cell.* Garland Science, 2000.

[14] Jain R., Pan J., Driscoll J.A., Wisner J.W., Huang T., Gunsten S.P. *et al.* Temporal relationship between primary and motile ciliogenesis in airway epithelial cells. *American Journal of Respiratory Cell and Molecular Biology*, 2010. 43(6):731–739.

[15] Salathe M. Regulation of mammalian ciliary beating. *Annual Review of Physiology*, 2007. 69:401–422.

[16] Woo K., Jensen-Smith H.C., Ludueña R.F. and Hallworth R. Differential synthesis of ß-tubulin isotypes in gerbil nasal epithelia. *Cell and Tissue Research*, 2002. 309(2):331–335.

[17] Jensen-Smith H.C., Ludueña R.F. and Hallworth R. Requirement for the ßi and ßiv tubulin isotypes in mammalian cilia. *Cell Motility and the Cytoskeleton*, 2003. 55(3):213–220.

[18] Pedersen L.B. and Rosenbaum J.L. Chapter two intraflagellar transport (ift): role in ciliary assembly, resorption and signalling. *Current topics in developmental biology*, 2008. 85:23–61.

[19] Stewart C.E., Torr E.E., Mohd Jamili N.H., Bosquillon C. and Sayers I. Evaluation of differentiated human bronchial epithelial cell culture systems for asthma research. *Journal of allergy*, 2012. 2012.

[20] Davenport J.R. and Yoder B.K. An incredible decade for the primary cilium: a look at a once-forgotten organelle. *American Journal of Physiology-Renal Physiology*, 2005. 289(6):F1159–F1169.

[21] Yu X., Ng C.P., Habacher H. and Roy S. Foxj1 transcription factors are master regulators of the motile ciliogenic program. *Nature genetics*, 2008. 40(12):1445–1453.

[22] Ostrowski L.E., Blackburn K., Radde K.M., Moyer M.B., Schlatzer D.M., Moseley A. *et al.* A proteomic analysis of human cilia identification of novel components. *Molecular & Cellular Proteomics*, 2002. 1(6):451–465.

[23] Grizzi F., Chiriva-Internati M., Franceschini B., Bumm K., Colombo P., Ciccarelli M. *et al.* Sperm protein 17 is expressed in human somatic ciliated epithelia. *Journal of Histochemistry & Cytochemistry*, 2004. 52(4):549–554.

[24] Jones C.J. *Epithelia: Advances in Cell Physiology and Cell Culture*. Kluwer Academic Publishers, 1990.

[25] Rock J.R., Onaitis M.W., Rawlins E.L., Lu Y., Clark C.P., Xue Y. *et al.* Basal cells as stem cells of the mouse trachea and human airway epithelium. *Proceedings of the National Academy of Sciences*, 2009. 106(31):12771–12775.

[26] Stripp B.R. and Reynolds S.D. Maintenance and repair of the bronchiolar epithelium. *Proceedings of the American Thoracic Society*, 2008. 5(3):328.

[27] Reynolds S.D. and Malkinson A.M. Clara cell: progenitor for the bronchiolar epithelium. *The international journal of biochemistry & cell biology*, 2010. 42(1):1–4.

[28] Scholzen T. and Gerdes J. The ki-67 protein: from the known and the unknown. *Journal of cellular physiology*, 2000. 182(3):311–322.

[29] Rose D., Maddox P. and Brown D. Which proliferation markers for routine immunohistology? a comparison of five antibodies. *Journal of clinical pathology*, 1994. 47(11):1010–1014.

[30] Nawijn M.C., Hackett T.L., Postma D.S., van Oosterhout A.J. and Heijink I.H. E-cadherin: gatekeeper of airway mucosa and allergic sensitization. *Trends in immunology*, 2011. 32(6):248–255.

[31] Berx G., Becker K.F., Höfler H. and Van Roy F. Mutations of the human e-cadherin (cdh1) gene. *Human mutation*, 1998. 12(4):226–237.

[32] Boitano S., Sanderson M.J. and Dirksen E.R. A role for ca (2+)-conducting ion channels in mechanically-induced signal transduction of airway epithelial cells. *Journal of cell science*, 1994. 107(11):3037–3044.

[33] Celli B., MacNee W., Agusti A., Anzueto A., Berg B., Buist A. *et al.* Standards for the diagnosis and treatment of patients with copd: a summary of the ats/ers position paper. *European Respiratory Journal*, 2004. 23(6):932–946.

[34] Chung K. *Airway Smooth Muscle in Asthma and COPD: Biology and Pharmacology*. Wiley, 2008.

[35] World health organization: Chronic obstructive pulmonary disease (copd), 2012. URL `http://www.who.int/respiratory/copd/en/`.

[36] World health organization: Asthma, 2013. URL `http://www.who.int/mediacentre/factsheets/fs307/en/index.html`.

[37] Coraux C., Hajj R., Lesimple P. and Puchelle E. In vivo models of human airway epithelium repair and regeneration. *European Respiratory Review*, 2005. 14(97):131–136.

[38] Montefort S., Roberts J., Beasley R., Holgate S. and Roche W. The site of disruption of the bronchial epithelium in asthmatic and non-asthmatic subjects. *Thorax*, 1992. 47(7):499–503.

[39] Yu H., Li Q., Kolosov V.P., Perelman J.M. and Zhou X. Regulation of cigarette smoke-mediated mucin expression by hypoxia-inducible factor-1α via epidermal growth factor receptor-mediated signaling pathways. *Journal of Applied Toxicology*, 2012. 32(4):282–292.

[40] Di Y.P., Zhao J. and Harper R. Cigarette smoke induces muc5ac protein expression through the activation of sp1. *Journal of Biological Chemistry*, 2012. 287(33):27948–27958.

[41] Shaykhiev R., Otaki F., Bonsu P., Dang D.T., Teater M., Strulovici-Barel Y. *et al.* Cigarette smoking reprograms apical junctional complex molecular architecture in the human airway epithelium in vivo. *Cellular and Molecular Life Sciences*, 2011. 68(5):877–892.

[42] Heijink I.H., Brandenburg S.M., Postma D.S. and van Oosterhout A.J. Cigarette smoke impairs airway epithelial barrier function and cell–cell contact recovery. *European Respiratory Journal*, 2012. 39(2):419–428.

[43] Maunders H., Patwardhan S., Phillips J., Clack A. and Richter A. Human bronchial epithelial cell transcriptome: gene expression changes following acute exposure to whole cigarette smoke in vitro. *American Journal of Physiology-Lung Cellular and Molecular Physiology*, 2007. 292(5):L1248–L1256.

[44] Beisswenger C., Platz J., Seifart C., Vogelmeier C. and Bals R. Exposure of differentiated airway epithelial cells to volatile smoke in vitro. *Respiration*, 2004. 71(4):402–409.

[45] Mio T., Romberger D.J., Thompson A.B., Robbins R.A., Heires A. and Rennard S.I. Cigarette smoke induces interleukin-8 release from human bronchial epithelial cells. *American journal of respiratory and critical care medicine*, 1997. 155(5):1770–1776.

[46] Baggiolini M. and Clark-Lewis I. Interleukin-8, a chemotactic and inflammatory cytokine. *FEBS letters*, 1992. 307(1):97–101.

[47] Wang H., Liu X., Umino T., Skold C.M., Zhu Y., Kohyama T. *et al.* Cigarette smoke inhibits human bronchial epithelial cell repair processes. *American journal of respiratory cell and molecular biology*, 2001. 25(6):772–779.

[48] Coraux C., Martinella-Catusse C., Nawrocki-Raby B., Hajj R., Burlet H., Escotte S. *et al.* Differential expression of matrix metalloproteinases and interleukin-8 during regeneration of human airway epithelium in vivo. *The Journal of pathology*, 2005. 206(2):160–169.

[49] Ganesan S. and Sajjan U.S. Repair and remodeling of airway epithelium after injury in chronic obstructive pulmonary disease. *Current Respiratory Care Reports*, 2013. pages 1–10.

[50] Crosby L.M. and Waters C.M. Epithelial repair mechanisms in the lung. *American Journal of Physiology-Lung Cellular and Molecular Physiology*, 2010. 298(6):L715–L731.

[51] Chen P. and Parks W.C. Role of matrix metalloproteinases in epithelial migration. *Journal of cellular biochemistry*, 2009. 108(6):1233–1243.

[52] Legrand C., Gilles C., Zahm J.M., Polette M., Buisson A.C., Kaplan H. *et al.* Airway epithelial cell migration dynamics: Mmp-9 role in cell–extracellular matrix remodeling. *The Journal of cell biology*, 1999. 146(2):517–529.

[53] Buisson A.C., Zahm J.M., Polette M., Pierrot D., Bellon G., Puchelle E. *et al.* Gelatinase b is involved in the in vitro wound repair of human respiratory epithelium. *Journal of cellular physiology*, 1996. 166(2):413–426.

[54] BéruBé K., Aufderheide M., Breheny D., Clothier R., Combes R., Duffin R. *et al.* In vitro models of inhalation toxicity and disease. *Alternatives to Laboratory Animals*, 2009. 37(1):89–141.

[55] Lin H., Li H., Cho H.J., Bian S., Roh H.J., Lee M.K. *et al.* Air-liquid interface (ali) culture of human bronchial epithelial cell monolayers as an in vitro model for airway drug transport studies. *Journal of pharmaceutical sciences*, 2007. 96(2):341–350.

[56] Dvorak A., Tilley A.E., Shaykhiev R., Wang R. and Crystal R.G. Do airway epithelium air–liquid cultures represent the in vivo airway epithelium transcriptome? *American journal of respiratory cell and molecular biology*, 2011. 44(4):465.

[57] White S.R., Dorscheid D.R., Rabe K.F., Wojcik K.R. and Hamann K.J. Role of very late adhesion integrins in mediating repair of human airway epithelial cell monolayers after mechanical injury. *American journal of respiratory cell and molecular biology*, 1999. 20(4):787–796.

[58] Howat W.J., Holgate S.T. and Lackie P.M. Tgf-β isoform release and activation during in vitro bronchial epithelial wound repair. *American Journal of Physiology-Lung Cellular and Molecular Physiology*, 2002. 282(1):L115–L123.

[59] Malavia N.K., Raub C.B., Mahon S.B., Brenner M., Panettieri Jr R.A. and George S.C. Airway epithelium stimulates smooth muscle proliferation. *American journal of respiratory cell and molecular biology*, 2009. 41(3):297.

[60] Planus E., Galiacy S., Matthay M., Laurent V., Gavrilovic J., Murphy G. *et al.* Role of collagenase in mediating in vitro alveolar epithelial wound repair. *Journal of Cell Science*, 1999. 112(2):243–252.

[61] Lechapt-Zalcman E., Prulière-Escabasse V., Advenier D., Galiacy S., Charrière-Bertrand C., Coste A. *et al.* Transforming growth factor-β1 increases airway wound repair via mmp-2 upregulation: a new pathway for epithelial wound repair? *American Journal of Physiology-Lung Cellular and Molecular Physiology*, 2006. 290(6):L1277–L1282.

[62] Zahm J.M., Kaplan H., Hérard A.L., Doriot F., Pierrot D., Somelette P. *et al.* Cell migration and proliferation during the in vitro wound repair of the respiratory epithelium. *Cell motility and the cytoskeleton*, 1997. 37(1):33–43.

[63] Crespin S., Bacchetta M., Huang S., Dudez T., Wiszniewski L. and Chanson M. Approaches to study differentiation and repair of human airway epithelial cells. In *Cystic Fibrosis*, pages 173–185. Springer, 2011.

[64] Rodgman A. and Perfetti T.A. *The chemical components of tobacco and tobacco smoke.* CRC press, 2013.

[65] Keith C. and Tesh P. Measurement of the total smoke issuing from a burning cigarette. *Tobacco Science*, 1965. 9:61–64.

[66] Liu X., Conner H., Kobayashi T., Kim H., Wen F., Abe S. *et al.* Cigarette smoke extract induces dna damage but not apoptosis in human bronchial epithelial cells. *American journal of respiratory cell and molecular biology*, 2005. 33(2):121–129.

[67] Chiappara G., Gjomarkaj M., Virzi A., Sciarrino S., Ferraro M., Bruno A. *et al.* The role of p21 waf1/cip1 in large airway epithelium in smokers with and without copd. *Biochimica et Biophysica Acta (BBA)-Molecular Basis of Disease*, 2013.

[68] Hellermann G.R., Nagy S.B., Kong X., Lockey R.F. and Mohapatra S.S. Mechanism of cigarette smoke condensate-induced acute inflammatory response in human bronchial epithelial cells. *Respiratory research*, 2002. 3(1):22.

[69] Lavigne M.C. and Eppihimer M.J. Cigarette smoke condensate induces mmp-12 gene expression in airway-like epithelia. *Biochemical and biophysical research communications*, 2005. 330(1):194–203.

[70] Mathis C., Poussin C., Weisensee D., Gebel S., Hengstermann A., Sewer A. *et al.* Human bronchial epithelial cells exposed in vitro to cigarette smoke at the air-liquid interface resemble bronchial epithelium from human smokers. *American Journal of Physiology-Lung Cellular and Molecular Physiology*, 2013. 304(7):L489–L503.

[71] Phillips J., Kluss B., Richter A., Massey E. *et al.* Exposure of bronchial epithelial cells to whole cigarette smoke: assessment of cellular responses. *Alternatives to Laboratory Animals*, 2005. 33(3):239–48.

[72] Kaur N., Lacasse M., Roy J.P., Cabral J.L., Adamson J., Errington G. *et al.* Evaluation of precision and accuracy of the borgwaldt rm20s® smoking machine designed for in vitro exposure. *Inhalation toxicology*, 2010. 22(14):1174–1183.

[73] Lie Y.S. and Petropoulos C.J. Advances in quantitative pcr technology: 5' nuclease assays. *Current opinion in biotechnology*, 1998. 9(1):43–48.

[74] Heid C.A., Stevens J., Livak K.J. and Williams P.M. Real time quantitative pcr. *Genome research*, 1996. 6(10):986–994.

[75] Stevenson B.R., Anderson J.M. and Bullivant S. The epithelial tight junction: structure, function and preliminary biochemical characterization. *Molecular and cellular biochemistry*, 1988. 83(2):129–145.

[76] Balder R., Krunkosky T.M., Nguyen C.Q., Feezel L. and Lafontaine E.R. Hag mediates adherence of moraxella catarrhalis to ciliated human airway cells. *Infection and Immunity*, October 2009. 77(10):4597–4608.

[77] Pan J., You Y., Huang T. and Brody S.L. Rhoa-mediated apical actin enrichment is required for ciliogenesis and promoted by foxj1. *Journal of Cell Science*, 2007. 120(11):1868–1876.

[78] Wong A.P., Bear C.E., Chin S., Pasceri P., Thompson T.O., Huan L.J. *et al.* Directed differentiation of human pluripotent stem cells into mature airway epithelia expressing functional cftr protein. *Nat Biotech*, 2012. 30(9):876–882.

[79] Stewart C., Torr E., Jamili M., Nur H., Bosquillon C. and Sayers I. Evaluation of differentiated human bronchial epithelial cell culture systems for asthma research. *Journal of Allergy*, 2012. 2012:1–11.

[80] Turner J., Roger J., Fitau J., Combe D., Giddings J., Heeke G.V. *et al.* Goblet cells are derived from a foxj1-expressing progenitor in a human airway epithelium. *American Journal of Respiratory Cell and Molecular Biology*, 2011. 44(3):276–284.

[81] Delgado O., Kaisani A.A., Spinola M., Xie X.J., Batten K.G., Minna J.D. *et al.* Multipotent capacity of immortalized human bronchial epithelial cells. *PLoS ONE*, 2011. 6(7):e22023.

[82] Sajjan U., Wang Q., Zhao Y., Gruenert D.C. and Hershenson M.B. Rhinovirus disrupts the barrier function of polarized airway epithelial cells. *American Journal of Respiratory and Critical Care Medicine*, 2008. 178(12):1271–1281.

[83] Humlicek A.L., Manzel L.J., Chin C.L., Shi L., Excoffon K.J.D.A., Winter M.C. *et al.* Paracellular permeability restricts airway epithelial responses to selectively allow activation by mediators at the basolateral surface. *The Journal of Immunology*, 2007. 178(10):6395–6403.

[84] Banks-Schlegel S. and Green H. Involucrin synthesis and tissue assembly by keratinocytes in natural and cultured human epithelia. *The Journal of cell biology*, 1981. 90(3):732–737.

[85] Tanabe T., Kanoh S., Moskowitz W.B. and Rubin B.K. Cardiac asthmatransforming growth factor-03b2 and cardiac asthmatransforming growth factor-β from the failing heart leads to squamous metaplasia in human airway cells and in the murine lung. *CHEST Journal*, 2012. 142(5):1274–1283.

[86] Lotan R. Squamous cell differentiation markers in normal, premalignant, and malignant epithelium: effects of retinoids. *Journal of Cellular Biochemistry*, 1993. 53(S17F):167–174.

[87] Hong K.U., Reynolds S.D., Watkins S., Fuchs E. and Stripp B.R. Basal cells are a multipotent progenitor capable of renewing the bronchial epithelium. *The American journal of pathology*, 2004. 164(2):577–588.

[88] Chen P. and Moldoveanu S. Mainstream smoke chemical analyses for 2r4f kentucky reference cigarette. *Beiträge zur Tabakforshung International/Contributions to Tobacco Research*, 2003.

[89] Noonan E.J., Place R.F., Giardina C. and Hightower L.E. Hsp70b' regulation and function. *Cell stress & chaperones*, 2007. 12(4):393.

[90] Jauhiainen A., Thomsen C., Strömbom L., Grundevik P., Andersson C., Danielsson A. *et al.* Distinct cytoplasmic and nuclear functions of the stress induced protein ddit3/chop/gadd153. *PloS one*, 2012. 7(4):e33208.

[91] Das S.K., Sharma N.K., Hasstedt S.J., Mondal A.K., Ma L., Langberg K.A. *et al.* An integrative genomics approach identifies activation of thioredoxin/thioredoxin reductase-1-mediated oxidative stress defense pathway and inhibition of angiogenesis in obese nondiabetic human subjects. *Journal of Clinical Endocrinology & Metabolism*, 2011. 96(8):E1308–E1313.

[92] Minor L.K. *Handbook of assay development in drug discovery.* CRC Press, 2010.

[93] Humbert M., Durham S.R., Kimmitt P., Powell N., Assoufi B., Pfister R. *et al.* Elevated expression of messenger ribonucleic acid encoding il-13 in the bronchial mucosa of atopic and nonatopic subjects with asthma. *Journal of Allergy and Clinical Immunology*, 1997. 99(5):657–665.

Appendices

A Media

2x ALI medium

- · Bronchial Epithelial cell Basal Medium (BEBM), 250 ml (Lonza, CC-3171)
- · Bronchial Epithelial cell Growth Medium (BEGM), Single quots (Lonza, CC-4175), except Retionic acid (CC- 4085F)
- · BSA for 2x ALI (1.5 mg/ml), 500 µl

DMEM complete medium

- · Dulbecco's Modified Eagle Medium (DMEM), 500 ml (Gibco, 41965-039)
- · Minimum Essential Medium Non-Essential Amino Acids (MEM NEAA) 100X, 5 ml (Gibco, 11140-035)
- · Sodium Pyruvate (NaPyr) 100mM, 5 ml (Gibco, 11360-039)
- · L-Glutamine 200 mM, 5 ml (Gibco, 25030-024)

ALI medium ready-to-use

- · x ml DMEM complete medium
- · x ml 2x ALI medium
- · x µl Retionic acid (0.1 mM)

NHBE medium

- · Bronchial Epithelial cell Basal Medium (BEBM), 500 ml (Lonza, CC-3171)
- · Bronchial Epithelial cell Growth Medium (BEGM), Single quots (Lonza, CC-4175)

Bronchial Epithelial cell Growth Medium (BEGM) (Lonza, CC-4175)

- · Bovine Pituitary Extract 2 ml (Lonza, CC-4009F)
- · Insulin 0.5 ml (Lonza, CC-4021F)
- · Hydrocortisone 0.5 ml (Lonza, CC-4031F)
- · Gentamicin sulfate amphotericin-B -1000 0.5 ml (Lonza, CC-4081F)
- · Retionic acid 0.5 ml (Lonza, CC-4085F)
- · Transferrin 0.5 ml (Lonza, CC-4205F)
- · Triiodothyronine 0.5 ml (Lonza, CC-4211F)
- · Epinephrine 0.5 ml (Lonza, CC-4221F)
- · Human epidermal growth factor 0.5 ml (Lonza, CC-4230F)

BSA for 2x ALI (1.5 mg/ml)

· BSA (Sigma, A2153)
· NHBE medium

Retinoic acid 0.1 mM

· Retinoic acid (Sigma, R2625)
· DMSO (Sigma, D2438)

PureCol 3 µg/ml

· Purified bovine collagen solution 3 mg/ml (Advanced BioMatrix, 5005-B)
· Steril dd-H$_2$0

B   Dehydration of ALI cultures

Table B1: Dehydration of ALI cultures

Step	Reagent	Time
1	70% EtOH	30 min
2	80% EtOH	15 min
3	95% EtOH	30 min
4	95% EtOH	30 min
5	Abs 99% EtOH	30 min
6	Abs 99% EtOH	15 min
7	Abs 99% EtOH	15 min
8	Xylene	15 min
9	Xylene	15 min
10	Paraffin	45 min
11	Paraffin	45 min
12	Paraffin	30 min

C   Mayers Htx/Eosin staining

Table C1: Mayers Htx/Eosin staining

Step	Reagent	Time
1	Xylene	5 min
2	Xylene	5 min
3	Abs 99% EtOH	5 min
4	Abs 99% EtOH	5 min
5	95% EtOH	5 min
6	95% EtOH	5 min
7	Mayers Htx	8 min
8	H_2O	5 min
9	Eosin	5 min
10	70% EtOH	1 sec
11	95% EtOH	1 sec
12	95% EtOH	1 sec
13	Abs 99% EtOH	1 sec
14	Abs 99% EtOH	1 sec
15	Xylene	5 min
16	Xylene	5 min

D   TaqMan

D.1   RNA purification

Table D1: RNA purification

Step	Description	Volume [µl]	Time [s]	Vacuum [%]
-	Pre-wet all wells with RNA Purification Wash solution 1	40	-	-
1	Load samples	200	120	20
2	Add RNA Purification Wash Solution 1	500	120	20
3	Add RNA Purification Wash Solution 2	650	120	20
4	Add AbsoluteRNA Wash Solution and incubate	50	900	-
5	Add RNA Purification Wash Solution 2 and incubate	400	300	-
6	Removal of solutions	-	120	20
7	Add RNA Purification Wash Solution 2	300	120	20
8	Add RNA Purification Wash Solution 2	300	120	20
9	Pre-Elution Vacuum	-	300	90
10	Add Nucleic Acid Purification Elution Solution	100	120	20

Reagents

RNA Purification Wash Solution 1 (Applied biosystems, 4305891)
RNA Purification Wash Solution 2 (Applied biosystems, 4305890)
AbsoluteRNA Wash Solution (Applied biosystems, 4305545)
Nucleic Acid Purification Elution Solution (Applied biosystems, 4305893)

D.2   TaqMan assay mix

Table D2: TaqMan assay mix

	Control genes [µl/rxn]			Genes [µl/rxn]
	Beta actin	GAPDH	36B4	Gene Expression Assay
X2 Primers	5	5	5	5
FP 10 µM	-	0.1	-	-
RP 10 µM	-	0.1	-	-
Probe 20 µM	-	0.1	-	-
FP/RP mix 10 µM	-	-	0.4	-
Probe 5 µM	-	-	0.4	-
GE Assay Mix	0.5	-	-	0.5
H_2O	1.5	1.7	1.2	1.5
Total volume	7	7	7	7

E   Antibody evaluation
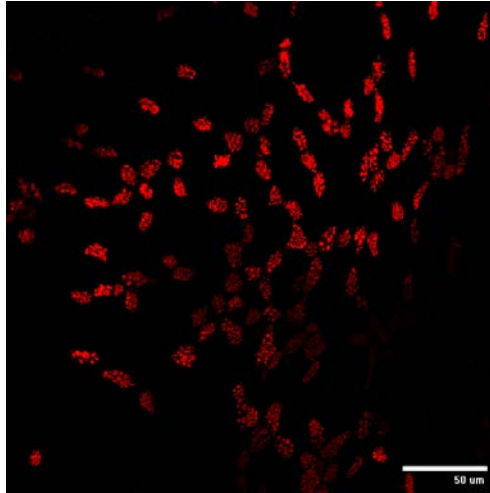
Figure E1: Immunofluorescent staining of ciliated cells through staining by SP17 (Sigma).
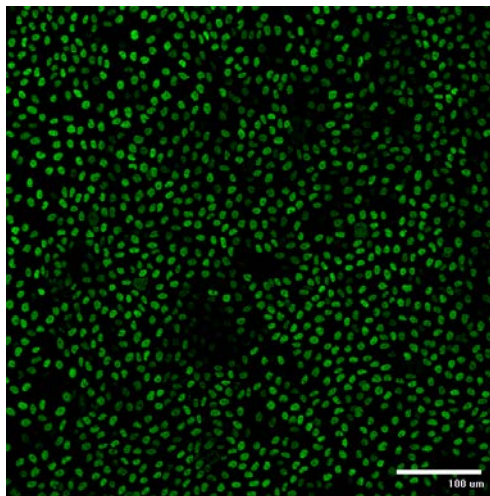

Figure E2: Immunofluorescent staining of basal cells through nuclear staining by p63 (Santa Cruz).
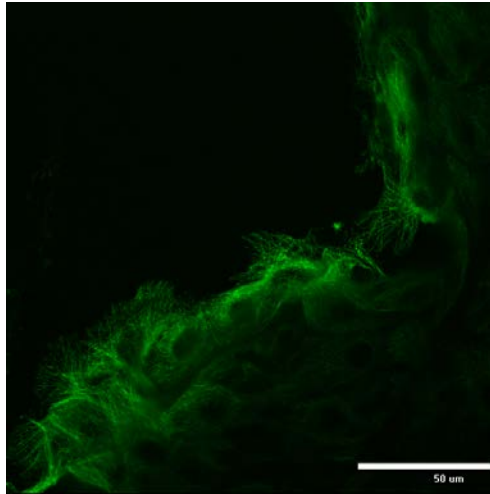
Figure E3: Immunofluorescent staining of cytoskeletal β_{IV}-tubulin through staining by TUBB4 (Novus).
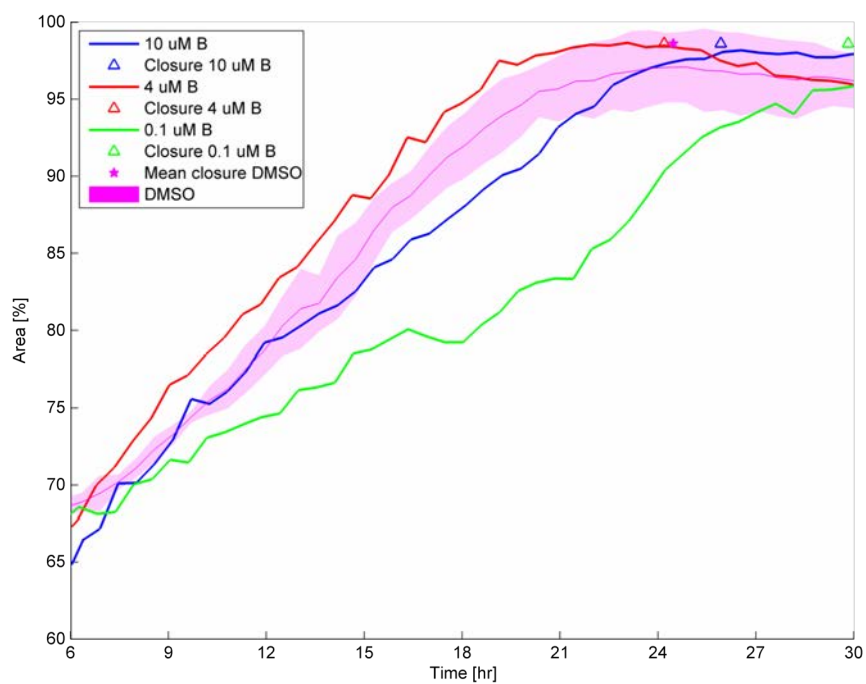
F   Compound treatment

Figure F1: Cell migration for cell culture treated with compound B, stars representing mean closure time and triangles each individual closing.
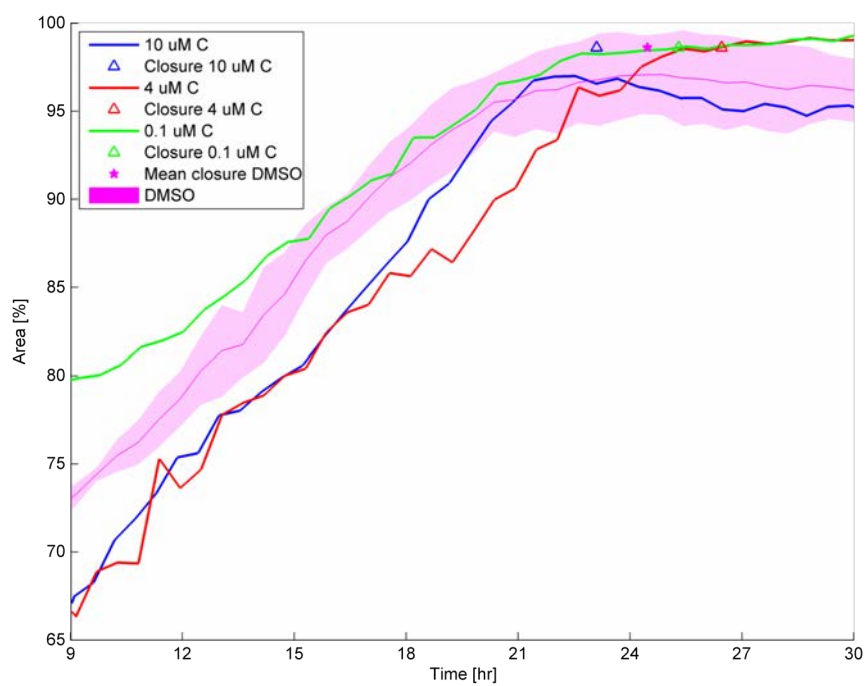
Figure F2: Cell migration for cell culture treated with positive control compound C, stars representing mean closure time and triangles each individual closing.